

# **First Search for Heavy Neutral Leptons with IceCube DeepCore**

**Dissertation**  
zur Erlangung des akademischen Grades  
doctor rerum naturalium  
(Dr. rer. nat.)

im Fach: Physik  
Spezialisierung: Experimentalphysik

eingereicht an der  
Mathematisch-Naturwissenschaftlichen Fakultät  
der Humboldt-Universität zu Berlin

von  
**Leander Fischer M. Sc.**  
geboren am 24. Oktober 1992  
in Heidelberg

Präsidentin der Humboldt-Universität zu Berlin  
Prof. Dr. Julia von Blumenthal

Dekanin der Mathematisch-Naturwissenschaftlichen Fakultät  
Prof. Dr. Caren Tischendorf

### **Copyright Notice**

This book is released into the public domain using the CC-BY-4.0 code.

To view a copy of the CC-BY-4.0 code, visit:

<https://creativecommons.org/licenses/by/4.0/>

### **Colophon**

This document was typeset with the help of KOMA-Script and L<sup>A</sup>T<sub>E</sub>X using the open-source kaobook template class.

The source code of this thesis is available at:

[https://github.com/LeanderFischer/phd\\_thesis](https://github.com/LeanderFischer/phd_thesis)

## **Zusammenfassung**

Zusammenfassung ...

## **Abstract**

Abstract ...



# Todo list

add fancy icecube header picture here (ORANGE) . . . . .	1
SB: there are more properties than just these. Somehow need a half sentence that explains why these are particularly important to single out (see ice papers for inspiration) (ORANGE) . . . . .	2
CL: maybe define that absorption and scattering lengths are? they are defined differently so this invites a comparison that is not so obvious (ORANGE) . . . . .	2
Add reference for the dust layer! Maybe also from the ice paper? mention/cite dust logger paper/procedure? (ORANGE) . . . . .	2
exchange for figure with scattering (check abs/sca is correct) (ORANGE) . . . . .	2
Add accuracy of the efficiency calibration here. (ORANGE) . . . . .	3
Blow up this image a bit, so it's better readable as marginfigure. (READ) . . . . .	3
CL: value? (YELLOW) . . . . .	4
SB: this needs revision. the energy range you mention is particular for oscillations already (atmopsheric neutrinos are plentiful outside of this range you mentioned). If you rewrite the first part you'll have to revisit the second part. Also in general I'd suggest not to rank analyses like Main and Other - DeepCore was orginally intended as a dark matter detector, and there are probably more DM analyses unblinded / year than oscillations. Just keep it general, no need to rank. (RED) . . . . .	4
Cite $n$ and $\theta_c$ (ORANGE) . . . . .	4
SB: you already mentioned that Cher. Rad. doesn't lead to significant energy loss. I suggest to clean up the text a bit, you dont' need to emphasize that so many times. Pick one place (probably here) and eliminate it elsewhere (RED) . . . . .	5
Add reference (PDG or find original) (ORANGE) . . . . .	5
Add reference for these processes. (ORANGE) . . . . .	6
cite em shower distribution (RED) . . . . .	6
gamma (from equation) is not defined (RED) . . . . .	6
Add angular profile plot (Summer agrees!) (create one based on Leif Rädel as Alex did) (RED) . . . . .	6
JVS: I would describe simulation sets you produced in past rather than present tense (ORANGE) . . . . .	9
Make my own DC string positions/distances plot version, viable for the margin? (YELLOW) . . . . .	9
Re-make plot with all energies (cascades and total, both samples (they are the same)) (RED) . . . . .	10
Re-make plot with all decay lengths (both samples) (RED) . . . . .	10
describe why these are shown to highlight some key aspect (uniformity in both energies to sample the whole space, decay length as a result of the z sampling etc..), also add this shortly to the caption (RED) . . . . .	10
again, describe what is shown and why this is interesting (e.g. energy distribution between the cascades, realistic exponential decay length distribtuion..) also add this to the captions shortly (RED) . . . . .	11
JVS: consider remaking figures at the native size so type size is consistent. Also, consider making the legend box semi-transparent so the lines do not obscure the text and markers. (ORANGE) . . . . .	13

Maybe decide if I want to handle git repo urls/references in a different way.. currently (without date+title) they look ugly in the margin, so I just state them as regular cites, but Cris gave me some other ideas on how to handle them.. (YELLOW) . . . . .	13
Re-make plot with 3 target masses and better labels/legends etc. (RED) . . . . .	14
SB: emphasize the cut-off/suppression (ORANGE) . . . . .	15
Add comparisons of SM cross-sections between NuXSSplMkr and genie? (YELLOW) . . . . .	15
Calculate max BRs or remove.. (RED) . . . . .	15
JVS: consider also writing down the (trivial) 2-body decay kinematics for completeness and consistency This transition is a bit jarring as it is (RED) . . . . .	16
JVS: The build-up of the weight expression is hard to follow without knowing where it's going. It may be better to start with the fact that the importance sampling weight is the ratio of PDFs, then write down each pdf, then drill down into each of the terms (basically, the standard "tell me what you're going to tell me, then tell me, then tell me what you told me" scheme). (RED) . . . . .	17
Combine low/high plots and remove all traces of the separation in the thesis (tables/text/etc.) (ORANGE) . . . . .	18
What is the message of these plots? Make it clear in the text and also in the captions. Potentially cut down to one or two and leave the rest or move them to the appendix. (RED) . . . . .	18
maybe I want a figure for this, or not so important? (YELLOW) . . . . .	19
Elaborate whether this is the case (show it in a plot?). Discuss directionality of cascades in general. (ORANGE) . . . . .	19
fix caption of this figure (RED) . . . . .	20
fix caption of this figure (RED) . . . . .	21
one half sentence on why this number was chosen? (ORANGE) . . . . .	22
make on figure, where the two selected regions are highlighted? (RED) . . . . .	24
fix caption (RED) . . . . .	24
re-make normalized? (ORANGE) . . . . .	25
fix caption (RED) . . . . .	25
re-make normalized? (ORANGE) . . . . .	25
fix caption (RED) . . . . .	25
circle back to the energy distributions I showed somewhere else, and state how the cascade energies are distributed in general (ORANGE) . . . . .	26
fix caption (RED) . . . . .	26
add table with cuts? (YELLOW) . . . . .	26
add example features? maybe like 2 or so? decay length and one other? (RED) . . . . .	27
fix caption of this figure (RED) . . . . .	27
fix caption (RED) . . . . .	27
Make a single plot, showing S/B or so? (RED) . . . . .	27
fix caption of this figure (RED) . . . . .	28
describe the "good fit" selection when I first show plots that use it (ORANGE) . . . . .	29
fix caption (RED) . . . . .	29

Check this number (RED) . . . . .	29
fix caption of this figure (RED) . . . . .	29
fix caption (RED) . . . . .	30
Check this number (RED) . . . . .	30
Make/add relevant plots here (RED) . . . . .	30
Plot energy (true total) and true decay length across the different levels (RED) . . . . .	30
Make table with the rates across the different levels for benchmark mass/mixing (RED) . . . . .	30
fix caption of this figure (RED) . . . . .	31
fix caption of this figure (RED) . . . . .	32
fix caption of this figure (RED) . . . . .	32
fix caption of this figure (RED) . . . . .	32



# Contents

<b>Abstract</b>	iii
<b>Contents</b>	ix
<b>1 The IceCube Neutrino Observatory</b>	<b>1</b>
1.1 Detector Components . . . . .	1
1.1.1 Digital Optical Modules and the Antarctic Ice . . . . .	2
1.1.2 IceCube . . . . .	3
1.1.3 DeepCore . . . . .	3
1.2 Particle Propagation in Ice . . . . .	4
1.2.1 Cherenkov Effect . . . . .	4
1.2.2 Energy Losses . . . . .	5
1.3 Event Morphologies . . . . .	7
<b>2 Heavy Neutral Lepton Signal Simulation</b>	<b>9</b>
2.1 Model Independent Simulation . . . . .	9
2.1.1 Simplistic Samples . . . . .	9
2.1.2 Realistic Sample . . . . .	10
2.2 Model Dependent Simulation . . . . .	12
2.2.1 Custom LeptonInjector . . . . .	12
2.2.2 Sampling Distributions . . . . .	16
2.2.3 Weighting Scheme . . . . .	17
2.2.4 Generation Level Distributions . . . . .	18
<b>3 Detecting Low Energetic Double Cascades</b>	<b>19</b>
3.1 Reconstruction . . . . .	19
3.1.1 Table-Based Minimum Likelihood Algorithms . . . . .	19
3.1.2 Optimization for Low Energy Events . . . . .	20
3.1.3 Performance . . . . .	22
3.2 Double Cascade Classification . . . . .	26
3.2.1 Classification Results . . . . .	27
3.3 Generic Double Cascade Performance . . . . .	29
3.3.1 Idealistic Events . . . . .	29
3.3.2 Realistic Events . . . . .	30
3.3.3 Selection Efficiency . . . . .	30
3.3.4 Performance . . . . .	30
<b>Bibliography</b>	<b>35</b>



# List of Figures

1.1	IceCube overview	1
1.2	IceCube sideview	2
1.3	Digital Optical Module (DOM)	3
1.4	IceCube top view	3
1.5	Cherenkov light front	5
2.1	DeepCore string spacing	10
2.2	Simplified model independent simulation generation level distributions	11
2.3	Realistic model independent simulation generation level distributions	12
2.4	HNL branching ratios	13
2.5	Custom HNL total cross-sections for the four target masses compared to the total ( $\nu_\tau/\bar{\nu}_\tau$ NC) cross-section used for SM neutrino simulation production with GENIE.	14
2.6	Model dependent simulation generation level distributions	18
3.2	short	21
3.3	Preliminary 2-d reconstructed versus true cascade energy resolutions	23
3.4	Preliminary 2-d reconstructed versus true decay length resolutions	24



# List of Tables

1.1	IceCube low energy event signatures and underlying interactions . . . . .	7
2.1	Simplified model independent simulation sampling distributions . . . . .	11
2.2	Realistic model independent simulation sampling distributions . . . . .	12
2.3	HNL mass dependent decay channels . . . . .	15
2.4	Model dependent simulation sampling distributions . . . . .	16



# The IceCube Neutrino Observatory

1

The IceCube Neutrino Observatory [1] is a cubic-kilometer, ice-Cherenkov detector located at the geographic South Pole. IceCube utilizes the Antarctic glacial ice as detector medium to observe neutrinos by measuring the Cherenkov light produced from secondary charged particles. It was deployed between 2006 and 2011 and has been taking data since the installation of the first modules. The primary goal of IceCube is the observation of astrophysical neutrinos as a telescope, but it can also be used to study fundamental particle physics properties by measuring atmospheric neutrinos as well as studying cosmic rays.

This chapter first describes the main- and sub-array of the detector and its detection module in Section 1.1, the propagation of particles through ice is explained in Section 1.2, and finally, the signatures that IceCube can observe of the different particles are introduced in Section 1.3.

add fancy icecube header	
1.1 Detector Components	1
1.2 Particle Propagation in	
Ice	4
1.3 Event Morphologies	7

[1]: Aartsen et al. (2017), "The IceCube Neutrino Observatory: instrumentation and online systems"

## 1.1 Detector Components

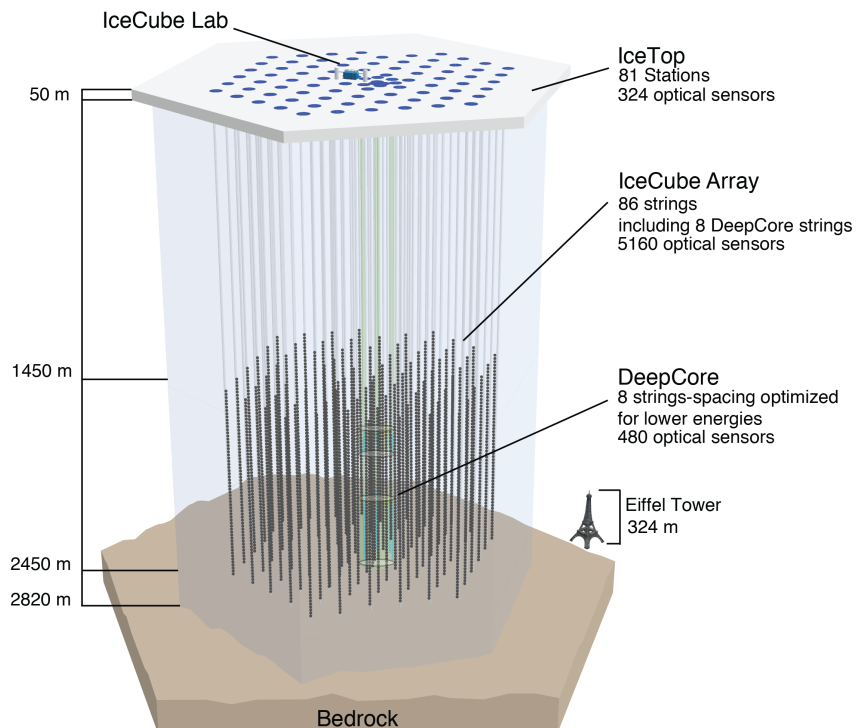


**Figure 1.1:** Overview of the IceCube detector showing the in-ice main- and sub-array IceCube and DeepCore, IceTop, and the IceCube Laboratory. From [1].

The full IceCube detector array consists of 86 vertical, in-ice strings and 81 surface stations as shown in Figure 1.1. The in-ice part is composed of 60 optical modules per string deployed at depths of 1450 m - 2450 m below the ice, while the surface stations of the cosmic air-shower array, *IceTop*, are ice-filled tanks. The surface stations and the majority of the strings are arranged in a hexagonal grid with the operations building, the *IceCube Laboratory* (ICL), central to the grid on the surface. A top view of the hexagonal arrangement

is shown in Figure 1.4. The in-ice array is designed to detect neutrinos in the energy range from GeV to PeV.

### 1.1.1 Digital Optical Modules and the Antarctic Ice

[2]: Price et al. (2000), "Age vs depth of glacial ice at South Pole"

SB: there are more properties than just these. Somehow need a half sentence that explains why these are particularly important to single out (see ice papers for inspiration) (ORANGE)

CL: maybe define that absorption and scattering lengths are? they are defined differently so this invites a comparison that is not so obvious (ORANGE)

[3]: Abbasi et al. (2022), "In-situ estimation of ice crystal properties at the South Pole using LED calibration data from the IceCube Neutrino Observatory"

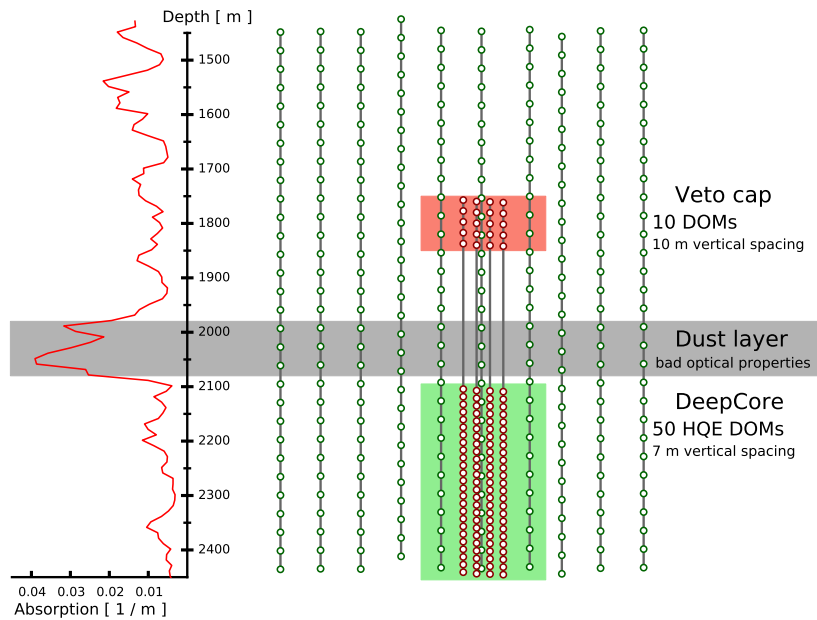
Add reference for the dust layer! Maybe also from the ice paper? mention Figure 1.4! (left panel) and the DOM positions around the dust layer. (ORANGE)

exchange for figure with scattering (check abs/sca is correct) (ORANGE)

[4]: Abbasi et al. (2009), "The IceCube data acquisition system: Signal capture, digitization, and timestamping"

[4]: Abbasi et al. (2009), "The IceCube data acquisition system: Signal capture, digitization, and timestamping"

The IceCube detection medium is the Antarctic glacial ice itself, which was formed over 100 000 years by accumulation of snow that was subsequently compressed by its own weight to form a dense crystal structure [2]. As a result of this formation process, the optical properties, scattering and absorption, primarily change with depth. Within the detector volume the absorption length ranges from 100 m - 400 m, while the scattering length lies between 20 m and 100 m. They are correlated, with the absorption length being roughly four times the scattering length [3]. The vertical distribution of scattering and absorption length can be seen in Figure 1.2, where one dominant feature is the *dust layer* between 2000 m and 2100 m depth. This region has a higher concentration of dust particles that were deposited in a period of high volcanic activity, which leads to bad optical properties in form of larger scattering and absorption.



The ice is instrumented by 5160 optical sensors called *Digital Optical Modules* (DOMs) [4], which can detect the Cherenkov light produced by charged particles traveling through the ice. Each DOM is made of a spherical glass housing, containing a downward-facing Photomultiplier Tube (PMT), the main-board with control, readout, and processing-electronics, and a LED flasher-board for calibration purposes. The design and the individual components of a DOM can be seen in Figure 1.3.

The majority of PMTs are the 10" Hamamatsu R7081-02, which have a bialkali photocathode and are sensitive to wavelengths in the range of 300 nm to 650 nm, with a peak quantum efficiency of 25% at 390 nm. In the central part of the IceCube array the peak efficiency reaches 34%. The dark count rate in the temperature range of  $-40^{\circ}\text{C}$  to  $-20^{\circ}\text{C}$  is  $\sim 300$  Hz. The DOM electronics measure the PMT voltage and control the gain. At a voltage crossing of the equivalent to 0.25 PE the waveform readout is activated [4]. Only when

either one of the nearest or next to nearest DOMs above or below also sees a voltage crossing within a  $1\text{ }\mu\text{s}$  time window<sup>1</sup>, the voltages are digitized and sent to the ICL. Through the application of a waveform unfolding algorithm, called *WaveDeform* [5], the waveforms are compressed, and the results are the reconstructed times and charges of the photo-electrons. This is the basis for all further IceCube data processing.

The PMT is covered with a mu-metal grid (made from wire mesh), shielding the photocathode from Earth's magnetic field, and it is optically coupled to the glass sphere by RTV silicone gel. The glass sphere is a pressure vessel, designed to withstand both the constant ice pressure and the temporary pressure during the refreezing process of the water in the drill hole during deployment (peaking at around 690 bar). The sphere is held by a harness that connects the DOMs along a string and also guides the cable beside them.

The flasher-board controls 12 LEDs that produce optical pulses with a wavelength of 405 nm [1]. The LEDs can be pulsed separately or in combination with variable output levels and pulse lengths. Using the known information of the light source positions and times this can be used for in-situ calibration of the detector by measuring absorption and scattering properties of the ice. Calibrating the absolute efficiency of the DOMs itself is more accurately done using minimum ionizing muons [6, 7], since the total amplitude of the LED light is not well known.

## 1.1.2 IceCube

The 78 strings that are arranged in a hexagonal pattern from the main part of the in-ice array, which is called *IceCube*. With a  $\sim 125\text{ m}$  horizontal spacing between the strings and a  $\sim 17\text{ m}$  vertical spacing between DOMs, IceCube has a lower energy threshold of around  $100\text{ GeV}$ . IceCube was designed to detect astrophysical neutrinos with energies above  $1\text{ TeV}$ .

The coordinate system that is used in IceCube is centered at  $46500^\circ\text{E}, 52200^\circ\text{N}$  at an elevation of  $883.9\text{ m}$  [1]. Per definition, it's a right-handed coordinate system where the y-axis points along the Prime Meridian (Grid North) towards Greenwich, UK, and the x-axis points  $90^\circ$  clockwise from the y-axis (Grid East). The z-axis is normal to the ice surface, pointing upwards. For IceCube analyses depth is defined as the distance along the z axis from the ice surface, assumed to be at an elevation of  $2832\text{ m}$ .

## 1.1.3 DeepCore

The additional 8 strings form a denser sub-array of IceCube called *DeepCore* [8]. It's located at the bottom-center of the in-ice array and its *fiducial volume* also includes the 7 surrounding IceCube strings as shown in Figure 1.4. The strings in this region have a closer average horizontal distance of about  $70\text{ m}$ . The lower 50 DeepCore DOMs on each string are placed in the region of clear ice below the dust layer between  $2100\text{ m}$  to  $2450\text{ m}$  depth, where their vertical spacing is  $\sim 7\text{ m}$ . The remaining 10 modules on each string are placed above the dust layer to be used as veto against atmospheric muons as can be seen in Figure 1.2. Additionally, the DeepCore DOMs are equipped with higher quantum efficiency PMTs. The combination of the denser spacing, the high

<sup>1</sup>: This is referred to as a *hard local coincidence (HLC)* [4].

[5]: Aartsen et al. (2014), "Energy Reconstruction Methods in the IceCube Neutrino Telescope"

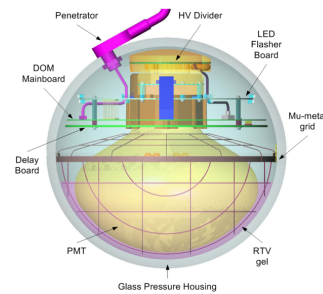


**Figure 1.3:** Design and components of a Digital Optical Module (DOM) [4]

[1]: Aartsen et al. (2017), "The IceCube Neutrino Observatory: instrumentation and online systems"

[6]: Feintzeig (2014), "Searches for Point-like Sources of Astrophysical Neutrinos with the IceCube Neutrino Observatory"

[7]: Kulacz (2019), "In Situ Measurement of the IceCube DOM Efficiency Factor Using Atmospheric Minimum Ionizing Muons"

Add accuracy of the efficiency calibration here. (ORANGE)

[1]: Aartsen et al. (2017), "The IceCube Neutrino Observatory: instrumentation and online systems"

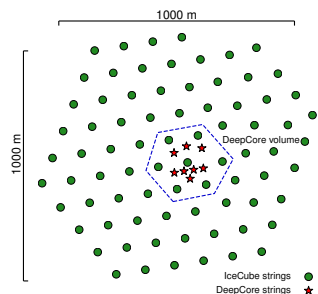


**Figure 1.4:** Top view of the IceCube array.

Blow up this image a bit, so it's better readable as marginfigure. (READ)

[8]: Abbasi et al. (2012), "The design and performance of IceCube DeepCore"

CL: value? (YELLOW)

SB: this needs revision.  
the energy range you  
mention is particular for  
oscillations already (at-  
mospheric neutrinos are  
plentiful outside of this  
range you mentioned).  
If you rewrite the first  
part you'll have to revisit  
the second part. Also in  
general I'd suggest not to  
rank analyses like Main  
and Other - DeepCore  
was originally intended  
as a dark matter detec-  
tor, and there are prob-  
ably more DM analyses  
unblinded / year than  
oscillations. Just keep it  
general, no need to rank.  
(RED)

[9]: Cherenkov (1937), "Visible Radiation Produced by Electrons Moving in a Medium with Velocities Exceeding that of Light"

quantum efficiency modules, and the most favorable ice properties below the dust layer leads to a lower energy detection threshold of around 5 GeV, allowing the more efficient observation of atmospheric neutrinos, which are mostly in the energy range of 10 GeV - 100 GeV. The main analysis performed with DeepCore is an atmospheric neutrino oscillation measurement, but the large flux of atmospheric neutrinos allows for many other Beyond Standard Model searches, such as searches for dark matter, non-standard interactions, or sterile neutrinos.

## 1.2 Particle Propagation in Ice

Neutrinos interacting in the ice via DIS produce muons, electromagnetic showers, and hadronic showers, depending on their flavor and the interaction type. The particles produced in those processes mainly lose their energy through *ionization*, *bremsstrahlung*, *pair production*, and the *photo-nuclear interaction*. Electrically charged particles also emit Cherenkov light when traveling through the ice, which is the main observable in IceCube, but only contributes a small amount to the total energy loss. The Cherenkov effect and the energy losses of the particles are described in the following sections, followed by an overview of the different particle signatures in IceCube.

### 1.2.1 Cherenkov Effect

When a charged particle moves through a medium with a velocity that is greater than the speed of light in that medium, it emits Cherenkov radiation, losing a very small amount of energy ( $\mathcal{O}(10^{-4})$  of the total energy loss). The detection principle of IceCube DeepCore, is based on the observation of resulting Cherenkov photons that are emitted by the charged secondary particles produced in the neutrino interactions that were introduced in Section ???. The Cherenkov effect was first observed by Pavel Cherenkov in 1934 [9] and occurs when the charged particle travels faster than the phase velocity of light, therefore polarizing the medium. Upon de-excitation the molecules emit the received energy as photons in a spherical wavefront. Since the particle moves past this wavefront, the superposition of the spherical light emissions forms a cone, which is shown in blue in the bottom panel of Figure 1.5.

Using trigonometry, the angle  $\theta_c$  at which the Cherenkov light is emitted can be calculated as

$$\theta_c = \arccos\left(\frac{1}{\beta n}\right), \quad (1.1)$$

where  $\beta$  is the velocity of the particle in units of the speed of light and  $n$  is the refractive index of the medium. When the particle velocity is close to the speed of light, the equation holds and the angle is only dependent on the refractive index of the medium. For the Antarctic ice, the refractive index is  $n \approx 1.3$  and as a result  $\theta_c \approx 41^\circ$ .

The frequency of the emission depends on the charge  $z$  and the wavelength-dependent index of refraction  $n(\omega)$  and is given by the Frank-Tamm formula [10, 11]

$$\frac{d^2N}{dx d\lambda} = \frac{2\pi\alpha z^2}{\lambda^2} \left(1 - \frac{1}{\beta^2 n(\omega)^2}\right), \quad (1.2)$$

with  $\alpha \approx 1/137$  the fine structure constant,  $\lambda$  the wavelength of the emitted light, and  $x$  the path length traversed by the particle. Relativistic particles in ice produce roughly 250 photons per cm in the wavelength range of 300 nm - 500 nm [12].

## 1.2.2 Energy Losses

Even though relativistic, charged particles traveling through matter produce Cherenkov radiation, their energy is mainly lost through other processes that are dependent on the particle type and energy. The exact principles of energy loss for the different types can broadly be categorized into the three groups: quasi-continuous energy loss by muons, electromagnetic cascades, and hadronic cascades.

### Muons

Muons lose their energy by ionization, bremsstrahlung, pair production, and the photo-nuclear effect. The energy loss by ionization is the dominant process for muons above 1 GeV and has a weak energy dependence given by

$$\left\langle -\frac{dE}{dx} \right\rangle = a_I(E) + b_R(E) \cdot E , \quad (1.3)$$

where  $E$  is the energy and  $a_I(E)$  and  $b_R(E) \cdot E$  are the energy loss by ionization and the combined radiative losses, respectively. In the energy range relevant for this work (10 GeV - 100 GeV), the parameters  $a_I$  and  $b_R$  only depend on energy very weakly and can be approximated by constants. The energy loss is then given by

$$\left\langle -\frac{dE}{dx} \right\rangle = a + b \cdot E . \quad (1.4)$$

Based on this description, there is a critical energy which divides the regimes where ionization and radiative losses dominate. The critical energy is given by  $E_{\text{crit}} = a/b$  and for muons in ice it is  $\sim 713$  GeV (using  $a \approx 2.59 \text{ MeVcm}^{-1}$  and  $b \approx 3.63 \times 10^{-6} \text{ cm}^{-1}$  [13]). Since the energy range of interest is well below this critical energy, the range of a muon can easily be related to its energy by

$$\langle L \rangle = \frac{E_0}{a} . \quad (1.5)$$

Measuring the length of a muon track therefore allows for an estimation of its energy if the full track is contained within the instrumented volume of IceCube. Using the given numbers a 30 GeV muon travels  $\sim 116$  m, which is well within the instrumented volume of IceCube, which spans across distances of up to 1000 m. This approximate treatment does not take into account the stochastic nature of some energy losses. Bremsstrahlung and photo-nuclear interactions for example rarely occur, but when they do, they deposit a large chunk of energy. A thorough investigation of the energy losses of muons in ice can be found in [14].

### Electromagnetic Showers

Photons as well as electrons and positrons are produced either directly in neutrino interactions or in secondary particle interactions. Above a critical

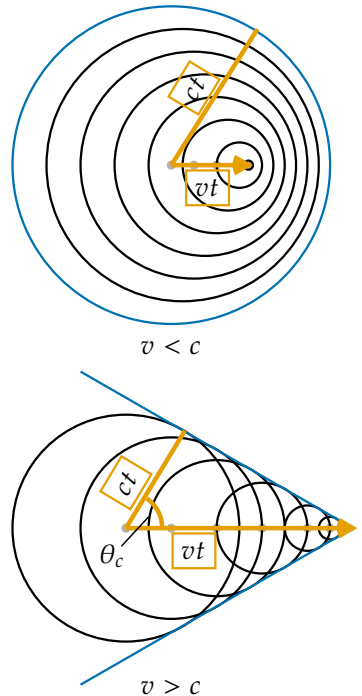


**Figure 1.5:** Schematic depiction of the spherical light front produced by a particle traveling slower than the speed of light in the medium (top) and the formation of the Cherenkov light front produced by a charged particle traveling faster than the speed of light in the medium (bottom). Blue is the resulting wavefront, while the black circles are spherically emitted light at each position and the orange arrows show the direction of the particle.

#### Cite $n$ and $\theta_c$ (ORANGE)

[10]: Frank et al. (1937), "Coherent visible radiation from fast electrons passing through matter"

[11]: Tamm (1991), "Radiation Emitted by Uniformly Moving Electrons"

[12]: Rädel et al. (2012), "Calculation of the Cherenkov light yield from low energetic secondary particles accompanying high-energy muons in ice and water with Geant4 simulations"

SB: you already mentioned that Cher. Rad. doesn't lead to significant energy loss. I suggest to clean up the text a bit, you don't need to emphasize that so many times. Pick one place (probably here) and eliminate it elsewhere (RED)

Add reference (PDG or find original) (ORANGE)

[13]: Chirkin et al. (2004), "Propagating leptons through matter with Muon Monte Carlo (MMC)"

[14]: Raedel (2012), "Simulation Studies of the Cherenkov Light Yield from Relativistic Particles in High-Energy Neutrino Telescopes with Geant4"

Add reference for these processes. (ORANGE)

[15]: Tanabashi et al. (2018), "Review of Particle Physics"

cite em shower distribution (RED)

gamma (from equation) is not defined (RED)

[14]: Raedel (2012), "Simulation Studies of the Cherenkov Light Yield from Relativistic Particles in High-Energy Neutrino Telescopes with Geant4"

[16]: Agostinelli et al. (2003), "Geant4—a simulation toolkit"

Add angular profile plot (Summer agrees!) (create one based on Leif Rädel as Alex did) (RED)

energy  $E_c$ , they lose their energy through repeated pair production and bremsstrahlung emission forming an expanding, electromagnetic shower profile. The particles' energy reduces with every interaction and their number increases until they fall below the critical energy where ionization and excitation of surrounding atoms become the dominant energy loss processes for electrons and positrons. For photons the remaining energy is lost through the Compton effect and the photoelectric effect. Below the critical energy no new shower particles are produced. Electromagnetic cascades can be characterized by the radiation length,  $X_0$ , after which electrons/positrons reduced their energy to  $1/e$  of their initial energy. For photons, it's equivalent to  $7/9$  of the mean free path of pair production. The critical energy for ice is  $E_c \approx 78$  MeV, with a radiation length of  $X_0 \approx 39.3$  cm [15].

The radiation length governs the longitudinal shower profile and using  $t = x/X_0$ , the shower intensity can be described by

$$\frac{dE}{dt} = E_0 b \frac{(bt)^{a-1} e^{-bt}}{\Gamma(a)}, \quad (1.6)$$

where  $a$  and  $b$  are parameters that have to be estimated from experiment. Based on the work from [14], performed with Geant4 [16], the parameters for electromagnetic showers in ice are

$$e^- : a \approx 2.01 + 1.45 \log_{10}(E_0/\text{GeV}), b \approx 0.63 , \quad (1.7a)$$

$$e^+ : a \approx 2.00 + 1.46 \log_{10}(E_0/\text{GeV}), b \approx 0.63 , \quad (1.7b)$$

$$\gamma : a \approx 2.84 + 1.34 \log_{10}(E_0/\text{GeV}), b \approx 0.65 . \quad (1.7c)$$

The maximum of the shower is at  $t_{max} = (a - 1)/b$  and the Cherenkov emission of the charged particles produced in the shower is peaked around the Cherenkov angle, since they are produced in the forward direction.

## Hadronic Showers

In DIS interactions, a cascade is always produced by the hadrons coming from the breaking target nucleus. The cascade is a result of secondary particles produced in strong interactions between the hadrons and the traversed matter. The charged particles produced in the shower will emit Cherenkov radiation, while neutral particles will be invisible to the detector. There is also an electromagnetic component of the shower, due to for example the decay of neutral pions into photons. Hadronic showers of the same energy as electromagnetic showers have larger fluctuations in energy deposition and shape, since they depend on the produced particle types. Hadrons also have a higher energy threshold for Cherenkov light production, because of their higher mass. Based on [14, 17], the visible electromagnetic fraction of hadronic showers can be parameterized as

$$F(E_0) = \frac{T_{\text{hadron}}}{T_{\text{EM}}} = 1 - (1 - f_0) \left( \frac{E_0}{E_s} \right)^{-m} , \quad (1.8)$$

where  $T_{\text{hadron/EM}}$  is the total track length of a hadronic/electromagnetic shower with the same energy,  $f_0$  is the ratio of hadronic and electromagnetic light yield,  $E_0$  is the initial energy, and  $E_s$  is an energy scale. The parameter  $m$  is a free model parameter. The ratio  $F(E_0)$  increases with energy, but is

[14]: Raedel (2012), "Simulation Studies of the Cherenkov Light Yield from Relativistic Particles in High-Energy Neutrino Telescopes with Geant4"

[17]: Gabriel et al. (1994), "Energy dependence of hadronic activity"

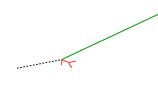
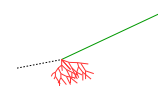
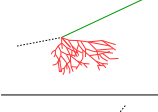
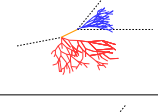
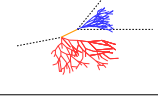
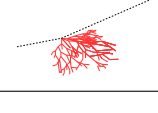
always smaller than 1. The variance of this distribution is given by

$$\sigma_F(E_0) = \sigma_0 \log(E_0)^{-\gamma}. \quad (1.9)$$

The parameters  $m$ ,  $E_s$ , and  $f_0$  were estimated by fitting the model to the results of Geant4 simulations. Cherenkov light from hadronic showers also peaks around the Cherenkov angle, but the angular distribution is more smeared out, due to the variations in particle type and their energy depositions.

### 1.3 Event Morphologies

The event morphologies produced by particles detected in IceCube are combinations of the three energy loss types described in Section 1.2.2, e.g. *cascades* from electromagnetic and hadronic showers and elongated *tracks* from muons traveling through the detector. Table 1.1 gives an overview of the possible event signatures.

Interaction	Secondary particles	Signature
CC $\nu_\mu^{(-)}$	 $\mu^\pm$ track	Track-only
	 $\mu^\pm$ track and hadrons	Cascade + track
CC $\nu_\tau^{(-)}$	 $\tau^\pm$ decaying into $\mu^\pm$ (~17% BR), hadrons	
	 $\tau^\pm$ decaying into $e^\pm$ or hadrons (~83% BR)	
CC $\nu_e^{(-)}$	 $e^\pm$ , hadrons	Cascade-only
NC $\nu_\ell^{(-)}$	 hadrons	

**Table 1.1:** IceCube low energy event signatures, their underlying interaction type, and the particles that produce them. Also shown are the secondary particles produced in the interactions. Black dashed lines represent neutrinos, green lines muons, orange line leptons, and blue and red lines are particles in electromagnetic and hadronic cascades, respectively. Adapted from [18].

**Neutrino** interactions are observed as cascades, tracks, or a combination of both, depending on the initial flavor and the interaction type for the specific event.

In  $\nu_\mu$ -CC interactions, a muon is produced in addition to a hadronic shower from the breaking nucleus. If the interaction happens outside the detector, but the muon passes through the detector, this will create a track-like signature. The same happens if the interaction happens inside, but the

energy transfer to the nucleus is small ( $y \approx 0$ ). At energies relevant for this work, tracks have length at the same order of the distance between DOMs, so they can be observed as such.

If the interaction happens inside the detector and the energy transfer to the hadronic part of the shower is larger, it will create a cascade with a track leaving it. A similar signature is observed after a  $\nu_\tau$  - CC interaction, in which a tau is produced that later decays into a muon, with a branching ratio of 17 %. In those cases the muon usually has a lower energy and the track will be fainter and harder to observe.

The other 83 % of  $\nu_\tau$  - CC interactions produce a tau that decays into an electron or hadrons, leaving a cascade-only signature through the electromagnetic or hadronic shower. All  $\nu_e$  - CC interactions also produce pure cascades, since the electron quickly loses its energy in an electromagnetic shower. In all  $\nu$  - NC interactions, the produced neutrino escapes and only the hadronic shower is observable. Since the size of the cascades at the energy range of interest is smaller than the spacing of the DOMs, they are approximately observed as point-like, spherical light sources. Even though the light is almost isotropically emitted, some asymmetry remains in the light profile, which can be used to reconstruct the direction of the incoming neutrino.

**Atmospheric muons** also produce pure track like signatures, similar to  $\nu_\mu$  - CC interactions happening outside the detector. They are one of the main backgrounds for analyses using atmospheric neutrinos and are therefore the target of many filter steps described in Section ??.

# Heavy Neutral Lepton Signal Simulation

# 2

The central part of this thesis is the HNL signal simulation itself. Since this is the first search for HNLs with IceCube DeepCore, there was no prior knowledge of the number of events expected per year nor of the expected performance in terms of reconstruction and classification accuracy which governs the 90 % confidence level on estimating the  $|U_{\tau 4}|^2$  mixing matrix element. This is the first HNL simulation developed for IceCube DeepCore. Two avenues of simulation generation were pursued in parallel. The physically accurate, model dependent simulation is described in Section 2.2 and a collection of model independent simulation samples was realized and is explained in Section 2.1. The latter is used for performance benchmarking and as a cross-check for the model dependent simulation. The SM simulation generation and the default low energy event selection and processing chain are introduced in Chapter ?? and everything but the generation is applied identically to both neutrinos and HNLs.

2.1	Model Independent Simulation . . . . .	9
2.2	Model Dependent Simulation . . . . .	12

## 2.1 Model Independent Simulation

JVS: I would describe simulation sets you produced in past rather than present tense (ORANGE)

To investigate the potential of IceCube to detect HNLs by identifying the unique double cascade morphology explained in Section ??, it is very valuable to have a simulation chain where the double cascade kinematics can be controlled directly. In a realistic model the decay kinematics and the absolute event expectation all depend on the specific model parameters chosen (see Section ??). To decouple the simulation from a specific parameter choice, a model independent double cascade generator was developed. Using this generator several simulation samples were produced to investigate the performance of IceCube DeepCore to detect low energetic double cascades, dependent on their properties. All samples are produced using a collection of custom generator functions [19] that place two EM cascade vertices with variable energy and direction at choosable locations in the detector. The results of this study will be discussed in Chapter 3.

### 2.1.1 Simplistic Samples

Make my own DC string positions/distances plot version, viable for the margin? (YELLOW)

To investigate some idealistic double cascade event scenarios, two samples are produced for straight up-going events that are centered on a string and horizontal events located inside DeepCore.

The first sample is used to investigate one of the most promising scenarios to detect a double cascade, where both cascade centers are located on a DeepCore string (namely string 81) and the directions are directly up-going. The horizontal positions and distances of all DeepCore fiducial volume strings are shown in Figure 2.1 and string 81 is at a medium distance of  $\sim 70$  m to its neighboring strings. As already mentioned in Section 1.1.3, DeepCore strings have higher quantum efficiency DOMs and a denser vertical spacing, making them better to detect low energetic events that produce little light. To produce the events, the  $x, y$  position of the cascades is fixed to the

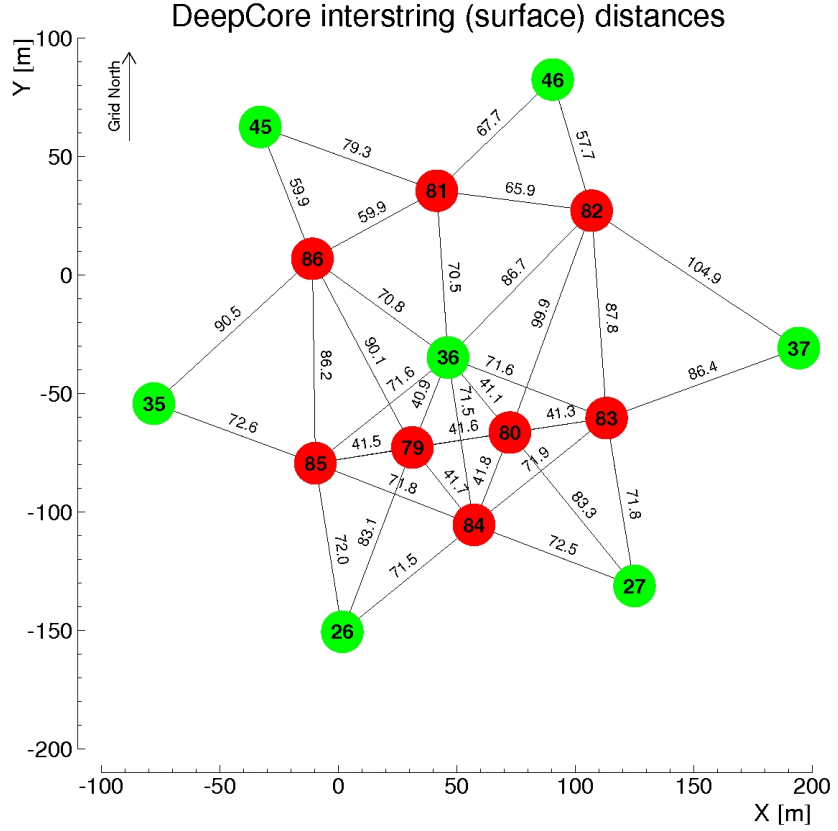


**Figure 2.1:** Horizontal positions and distances between DeepCore strings. Red strings are instrumented more densely (vertically) and partially have higher quantum efficiency (HQE) DOMs.

center of string 81 while the  $z$  positions are each sampled uniformly along the axis of the string. Note here that this will therefore not produce a uniform length distribution between the cascades. The positions are defined in the IceCube coordinate system that was already introduced in Section 1.1.2. The energies are sampled uniformly between 0.0 GeV and 60.0 GeV. The specific sampling distributions/values for the cascades are listed in Table 2.1. The order of the cascades is chosen such that the lower one is first ( $t_0 = 0.0$  ns) and the upper one is second ( $t_1 = L/c$ ), assuming the speed of light  $c$  as speed of the heavy mass state, traveling between the two cascades.

The second sample is used to investigate the reconstruction performance for horizontal events, where the spacing between DOMs is much larger. The cascades are placed uniformly on a circle centered in DeepCore. The direction is always horizontal and azimuth is defined by the connecting vector of both cascade positions. The energies are again sampled uniformly between 0.0 GeV and 60.0 GeV and the detailed sampling distributions/values are also listed in Table 2.1. Some examples of the generation level distributions of the simplified samples are shown in Figure 2.2, while further distributions can be found in Figure ??.

## 2.1.2 Realistic Sample

To thoroughly investigate the potential of IceCube DeepCore to detect double cascade events, a more realistic simulation sample is produced that aims to be as close as possible to the expected signal simulation explained in Section 2.2, while still allowing additional freedom to control the double cascade kinematics. For this purpose the total energy is sampled from an

Re-make plot with all energies (cascades and total, both samples (they are the same)) (RED)

Re-make plot with all decay lengths (both samples) (RED)

describe why these are shown to highlight some key aspect (uniformity in both energies to sample the whole space, decay length as a result of the  $z$  sampling etc..), also add this shortly to the caption (RED)

Sample	Variable	Distribution	Range/Value
<b>Up-going</b>			
	energy	uniform	0.0 GeV to 60.0 GeV
	zenith	fixed	180.0°
	azimuth	fixed	0.0°
	x, y position	fixed	(41.6, 35.49) m
	z position	uniform	-480.0 m to -180.0 m
<b>Horizontal</b>			
	energy	uniform	0.0 GeV to 60.0 GeV
	zenith	fixed	90.0°
	azimuth	uniform	0.0° to 360.0°
	x, y position	uniform (circle)	c=(46.29, -34.88) m, r=150.0 m
	z position	fixed	-330.0 m

**Table 2.1:** Generation level sampling distributions and ranges/values of up-going and horizontal model independent simulation.

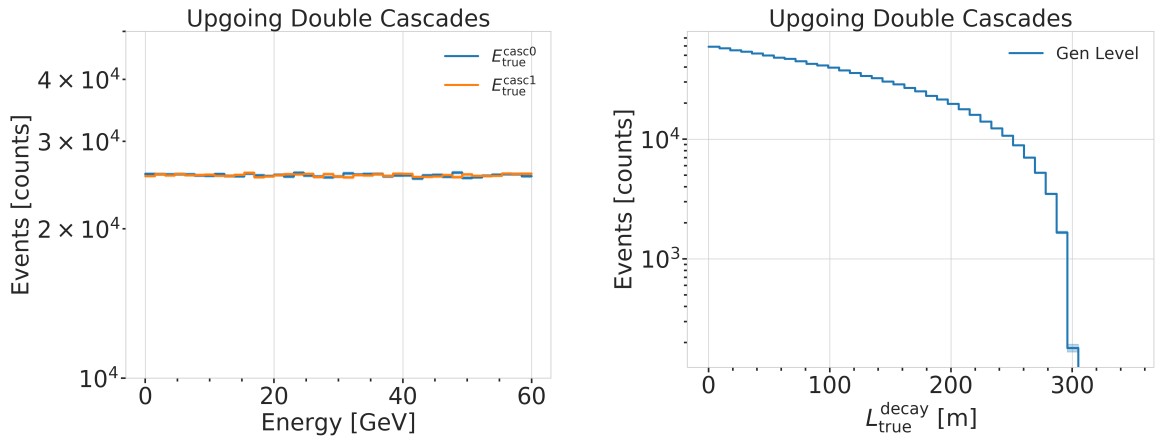


**Figure 2.2:** Generation level distributions of the simplistic simulation samples. Cascade and total energies (left) and decay lengths (right) of both samples are shown.

$E^{-2}$  power law, mimicking the energy spectrum of the primary neutrinos as stated in Section ???. The total energy is divided into two parts, by assigning a fraction between 0 % and 100 % to one cascade and the remaining part to the other cascade. This is a generic approximation of the realistic process described in Section 2.2, and chosen such that the whole sample covers various cases of energy distributions between the two cascades. To efficiently generate events in a way that produces distributions similar to what would be observed with DeepCore, one of the cascade positions is sampled inside the DeepCore volume by choosing its coordinates uniformly on a cylinder that is centered in DeepCore. This is similar to a trigger condition of one cascade always being inside the DeepCore fiducial volume. By choosing the direction of the event by sampling zenith and azimuth uniformly between 70° and 180° and 0° and 360°, respectively, the position of the other cascade can be inferred for a given decay length, assuming a travel speed of  $c$ , and choosing whether the cascade position that was sampled is the first cascade or the second with a 50 % chance. The decay length is sampled from an exponential distribution, as expected for a decaying heavy mass state. The sampling distributions/values are listed in Table 2.4. Example distributions of the generation level variables are shown in Figure 2.3, while further distributions can be found in Figure ??.

again, describe what is shown and why this is interesting (e.g. energy distribution between the cascades, realistic exponential decay length distribution..) also add this to the captions shortly (RED)

**Table 2.2:** Generation level sampling distributions and ranges/values of the realistic model independent simulation.

Variable	Distribution	Range/Value
energy (total)	power law $E^{-2}$	1 GeV to 1000 GeV
decay length	exponential $e^{-0.01L}$	0 m to 1000 m
zenith	uniform	70° to 180°
azimuth	uniform	0° to 360°
$x, y$ (one cascade)	uniform (circle)	$c=(46.29, -34.88)$ m, $r=150$ m
$z$ (one cascade)	uniform	-480.0 m to -180.0 m

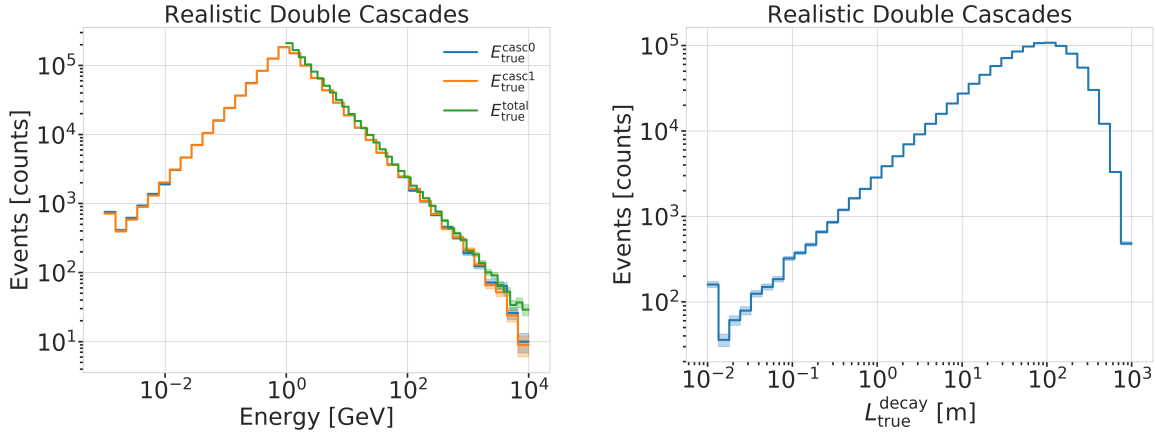


**Figure 2.3:** Generation level distributions of the simplistic realistic sample. Shown are the cascade and total energies (left) and decay lengths (right).

## 2.2 Model Dependent Simulation

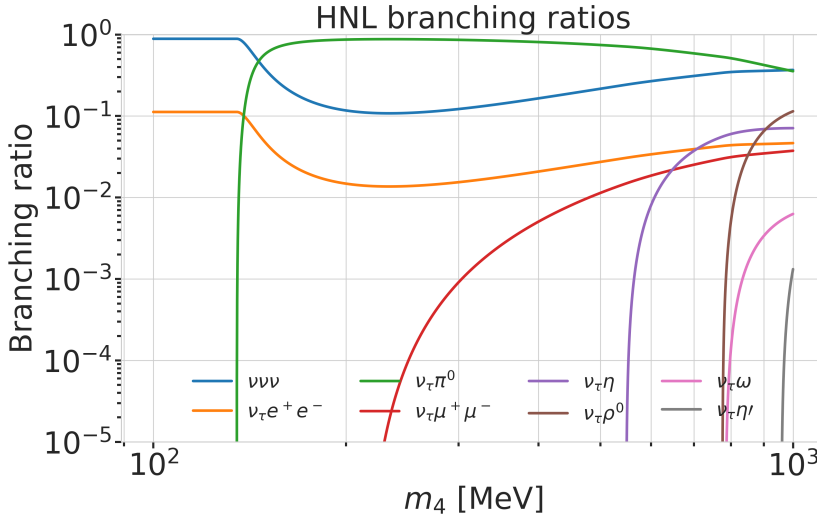
To estimate the HNL event expectation in IceCube DeepCore, depending on the specific model parameters, a generator was developed that is based on the HNL theory introduced in Section ???. For this work, only the interaction with the  $\tau$ -sector was taken into account ( $|U_{\alpha 4}^2| = 0$ ,  $\alpha = e, \mu$ ), which reduces the physics parameters of interest and relevant for the simulation to the fourth heavy lepton mass,  $m_4$ , and the mixing,  $|U_{\tau 4}^2|$ . The generator uses a customized *LeptonInjector* (LI) version to create the events and *LeptonWeighter* (LW) to weight them [20]. The modified LI and the essential components needed for the HNL simulation are described in the next sections, followed by the description of the weighting scheme and the sampling distributions chosen for the simulation generation.

[20]: Abbasi et al. (2021), “LeptonInjector and LeptonWeighter: A neutrino event generator and weighter for neutrino observatories”

### 2.2.1 Custom LeptonInjector

In its standard version, the LI generator produces neutrino interactions by injecting a lepton and a hadronic cascade at the interaction vertex of the neutrino, where the lepton is the charged (neutral) particle produced in a CC (NC) interaction and the cascade is the hadronic cascade from the breaking nucleus. The hadronic cascade is stored as a specific object of type *Hadrons*, which triggers the correct simulation of the shower development in the following simulation steps, identical to what will be described for SM neutrino simulation on Section ???. The main differences to an EM cascade is that part of the energy will not be observed, because it goes into neutral particles, and that the spatial development of the shower is different. Both objects are injected with the same  $(x, y, z, t)$  coordinates and the kinematics

are sampled from the differential and total cross-sections that are one of the inputs to LI.



JVS: consider remaking figures at the native size so type size is consistent. Also, consider making the legend box semi-transparent so the lines do not obscure the text and markers. (ORANGE)

**Figure 2.4:** Branching ratios of the HNL within the mass range considered in this work, only considering  $|U_{\tau 4}^2| \neq 0$ , calculated based on the results from [21].

In the modified version, the SM lepton at the interaction vertex is replaced by the new HNL particle, where the interaction cross-sections are replaced by custom, mass dependent HNL cross-sections. The HNL is forced to decay after a chosen distance<sup>1</sup> to produce secondary SM particles, where the decay mode is chosen with a probability given by the mass dependent branching ratios from the kinematically accessible decay modes shown in Figure 2.4. The cross-section and decay width calculations were implemented for this purpose and will be explained in more detail in the following. Another needed addition to LI is that the decay products of the HNL are also added to the list of MC particles in each event. They are injected with the correctly displaced position and delayed time from the interaction vertex, given the HNL decay length. These HNL daughter particles form the second cascade, not as a single hadronic cascade object, but as the explicit particles forming the shower. The kinematics of the two-body decays are computed analytically, while the three-body decay kinematics are calculated with MADGRAPH [22], which will also be explained further below. Independent of the number of particles in the final state of the HNL decay, the kinematics are calculated/simulated at rest and then boosted along the HNL momentum.

The injection is done using the LI *volume mode*, for the injection of the primary particle on a cylindrical volume, adding 50 % of the events with  $\nu_\tau$  and the other half with  $\bar{\nu}_\tau$  as primary particle types. The generator takes the custom double-differential/total cross-section splines described below and the parameters defining the sampling distributions as inputs.

### Cross-Sections

The cross-sections are calculated using the NuXSSPLMCR [23] software, which is a tool to calculate neutrino cross-sections from *parton distribution functions (PDFs)* and then fit to an N-dimensional tensor-product B-spline surface [24] to produce the splines that can be read and used with LI/LW. The tool was modified to produce the custom HNL cross-sections, where the main modification to calculate the cross-sections for the  $\nu_\tau$ -NC interaction into the new heavy mass state, is the addition of a kinematic condition to

1: The explicit sampling distributions and ranges can be found in Section 2.2.2.

[22]: Alwall et al. (2014), “The automated computation of tree-level and next-to-leading order differential cross sections, and their matching to parton shower simulations”

Maybe decide if I want to handle git repo urls/references in a different way.. currently (without date+title) they look ugly in the margin, so I just state them as regular cites, but Cris gave me some other ideas on how to handle them.. (YELLOW)

[24]: Whitehorn et al. (2013), “Penalized splines for smooth representation of high-dimensional Monte Carlo datasets”

[25]: Levy (2009), "Cross-section and polarization of neutrino-produced tau's made simple"

ensure that there is sufficient energy to produce the heavy mass state. It is the same condition fulfilled for the CC case, where the outgoing charged lepton mass is non-zero. Following [25] (equation 7), the condition

$$(1 + x\delta_N)h^2 - (x + \delta_4)h + x\delta_4 \leq 0 \quad (2.1)$$

is implemented for the NC case in the NuXSSplMkr code. Here

$$\delta_4 = \frac{m_4^2}{s - M^2}, \quad (2.2)$$

$$\delta_N = \frac{M^2}{s - M^2}, \text{ and} \quad (2.3)$$

$$h \stackrel{\text{def}}{=} xy + \delta_4, \quad (2.4)$$

with  $x$  and  $y$  being the Bjorken variables,  $m_4$  and  $M$  the mass of the heavy state and the target nucleon, respectively, and  $s$  the center of mass energy squared. The custom version was made part of the open source NuXSSplMkr software and can thus be found in [23]. The result of this kinematic condition is that events cannot be produced for energy,  $x$ ,  $y$  combinations that don't have sufficient energy going into the outgoing, massive lepton. This results in a reduction of the cross-section towards lower energies, which scales with the assumed mass of the HNL. This effect can clearly be seen in Figure 2.5.

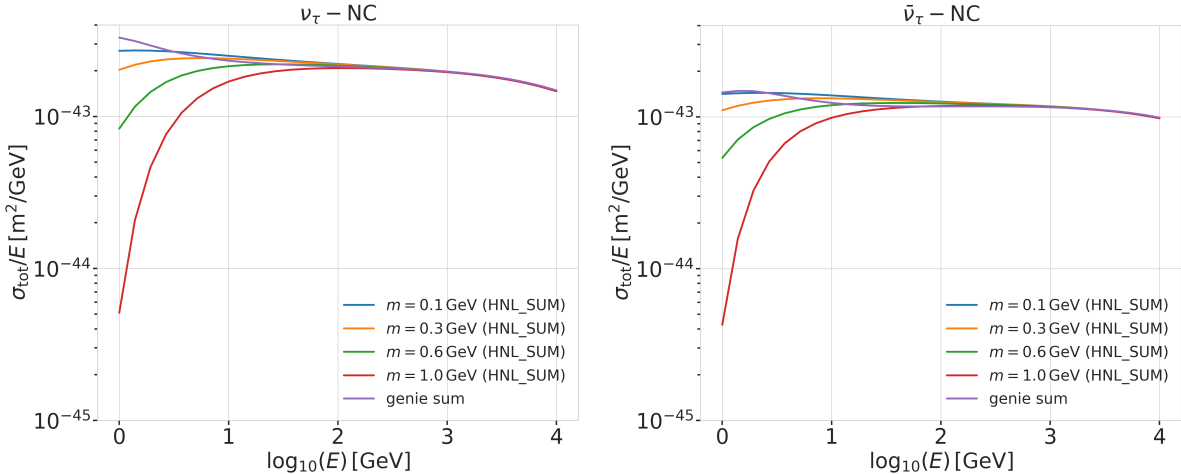


**Figure 2.5:** Custom HNL total cross-sections for the four target masses compared to the total ( $\nu_\tau/\bar{\nu}_\tau$  NC) cross-section used for SM neutrino simulation production with GENIE.

Re-make plot with 3 star  
get masses and better  
labels/legends etc. (RED)

The GRV98LO PDFs were added to the cross-section spline maker and used to create the HNL cross-sections for consistency with the SM neutrino simulation that will be explained in Section ???. The double-differential ( $d\sigma/dxdy$ ) and total ( $\sigma$ ) cross-sections were produced for the chosen target HNL masses and then splined in energy,  $x$ , and  $y$  and just in the energy, respectively. The produced cross-section are added to the custom LI version and used for the simulation generation and weighting. Figure 2.5 shows the total cross-sections that were produced compared to the cross-section used for the production of the SM  $\nu_\tau/\bar{\nu}_\tau$  NC background simulation. They agree above a certain energy ( $\sim 200$  GeV), where the modification should not have any effect on the cross-sections, which is the desired result of using the identical input PDFs and confirms that the unmodified cross-sections produced with NuXSSplMkr agree with the GENIE cross-sections, which

were used to generate the SM background MC.

## Decay Channels

The accessible decay channels are dependent on the mass of the HNL and the allowed mixing. For this analysis, where only  $|U_{\tau 4}|^2 \neq 0$ , the decay channels considered are listed in Table 2.3 and the corresponding branching ratios are shown in Figure 2.4. The individual branching ratio for a specific mass is calculated as  $\text{BR}_i(m_4) = \Gamma_i(m_4)/\Gamma_{\text{total}}(m_4)$ , where  $\Gamma_{\text{total}}(m_4) = \sum \Gamma_i(m_4)$ . The individual decay widths  $\Gamma_i$  are computed using the state-of-the-art calculations from [21], which are described in the following.

**2-Body Decay Widths** The decay to a neutral pseudoscalar meson is

$$\Gamma_{\nu_4 \rightarrow \nu_\tau P} = |U_{\tau 4}|^2 \frac{G_F^2 m_4^3}{32\pi} f_P^2 (1 - x_p^2)^2, \quad (2.5)$$

with  $x_P = m_P/m_4$  and the *effective decay constants*  $f_P$  given by

$$f_{\pi^0} = +0.1300 \text{ GeV}, \quad (2.6)$$

$$f_\eta = +0.0816 \text{ GeV}, \text{ and} \quad (2.7)$$

$$f_{\eta'} = -0.0946 \text{ GeV}, \quad (2.8)$$

while the decay to a neutral vector meson is given by

$$\Gamma_{\nu_4 \rightarrow \nu_\tau V} = |U_{\tau 4}|^2 \frac{G_F^2 m_4^3}{32\pi} \left( \frac{f_V}{m_V} \right)^2 g_V^2 (1 + 2x_V^2)(1 - x_V^2)^2, \quad (2.9)$$

with  $x_V = m_V/m_4$ ,

$$f_{\rho^0} = 0.171 \text{ GeV}^2, \quad (2.10)$$

$$f_\omega = 0.155 \text{ GeV}^2, \quad (2.11)$$

and

$$g_{\rho^0} = 1 - 2 \sin^2 \theta_w, \quad (2.12)$$

$$g_\omega = \frac{-2 \sin^2 \theta_w}{3}, \quad (2.13)$$

and  $\sin^2 \theta_w = 0.2229$  [26], where  $\theta_w$  is the Weinberg angle.

SB: emphasize the cut-off/suppression (ORANGE)

Add comparisons of SM cross-sections between NuXSSplMkr and genie? (YELLOW)

[21]: Coloma et al. (2021), “GeV-scale neutrinos: interactions with mesons and DUNE sensitivity”

Channel	Opens	$\hat{\text{BR}}$
$\nu_4 \rightarrow \nu_\tau \nu_\alpha \bar{\nu}_\alpha$	0 MeV	1.0
$\nu_4 \rightarrow \nu_\tau e^+ e^-$	1 MeV	?
$\nu_4 \rightarrow \nu_\tau \pi^0$	135 MeV	?
$\nu_4 \rightarrow \nu_\tau \mu^+ \mu^-$	211 MeV	?
$\nu_4 \rightarrow \nu_\tau \eta$	548 MeV	?
$\nu_4 \rightarrow \nu_\tau \rho^0$	770 MeV	?
$\nu_4 \rightarrow \nu_\tau \omega$	783 MeV	?
$\nu_4 \rightarrow \nu_\tau \eta'$	958 MeV	?

**Table 2.3:** Possible decay channels of the HNL, considering only  $|U_{\tau 4}|^2 \neq 0$ . Listed is the mass at which each channel opens and the maximum branching ratio.

Calculate max BRs or remove.. (RED)

[26]: Tiesinga et al. (2021), “CODATA recommended values of the fundamental physical constants: 2018”

**3-Body Decay Widths** The (invisible) decay to three neutrinos, one of flavor  $\tau$  and two of any flavor  $\alpha$ , is

$$\Gamma_{\nu_4 \rightarrow \nu_\tau \nu_\alpha \bar{\nu}_\alpha} = |U_{\tau 4}|^2 \frac{G_F^2 m_4^5}{192\pi^3}, \quad (2.14)$$

while the decay to two charged leptons (using  $x_\alpha = (m_\alpha/m_4)^2$ ) of the same flavor reads

$$\Gamma_{\nu_4 \rightarrow \nu_\tau l_\alpha^+ l_\alpha^-} = |U_{\tau 4}|^2 \frac{G_F^2 m_4^5}{192\pi^3} [C_1 f_1(x_\alpha) + C_2 f_2(x_\alpha)], \quad (2.15)$$

with the constants defined as

$$C_1 = \frac{1}{4}(1 - 4 \sin^2 \theta_w + 8 \sin^4 \theta_w), \quad (2.16)$$

$$C_2 = \frac{1}{2}(-\sin^2 \theta_w + 2 \sin^4 \theta_w), \quad (2.17)$$

the functions as

$$f_1(x_\alpha) = (1 - 14x_\alpha - 2x_\alpha^2 - 12x_\alpha^3)\sqrt{1 - 4x_\alpha} + 12x_\alpha^2(x_\alpha^2 - 1)L(x_\alpha), \quad (2.18)$$

$$f_2(x_\alpha) = 4[x_\alpha(2 + 10x_\alpha - 12x_\alpha^2)\sqrt{1 - 4x_\alpha} + 6x_\alpha^2(1 - 2x_\alpha + 2x_\alpha^2)L(x_\alpha)], \quad (2.19)$$

and

$$L(x) = \ln\left(\frac{1 - 3x_\alpha - (1 - x_\alpha)\sqrt{1 - 4x_\alpha}}{x_\alpha(1 + \sqrt{1 - 4x_\alpha})}\right). \quad (2.20)$$

### 3-Body Decay Kinematics with MadGraph

The specific MadGraph version used to produce the 3-body decay kinematics is `MADGRAPH4 v3.4.0` [27], which uses the decay diagrams calculated with `FEYNRULES 2.0` [28] and the Lagrangians derived in [21] as input. The *Universal FeynRules Output (UFO)* from `EFFECTIVE_HEAVYN_MAJORANA_v103` were used for our calculation. For each mass and corresponding decay channels, we produce  $1 \times 10^6$  decay kinematic variations in the rest frame and store those in a text file. During event generation, we uniformly select an event from that list, to simulate the decay kinematics of a 3-body decay.

### 2.2.2 Sampling Distributions

In principle, the generation level sampling distributions should be chosen such that at final level of the selection chain the phase space relevant for the analysis is covered with sufficient statistics to make a reasonable estimate of the event expectation. Initial distributions insufficiently covering the phase space leads to an underestimate of the expected rates, because part of the events that would pass the selection are not produced. This limits the expected analysis potential. Three discrete simulation samples were produced with HNL masses of 0.3 GeV, 0.6 GeV, and 1.0 GeV. Because during development it became clear that the low lengths component is crucial to get a reasonable event estimate, each sample consists of a part that is generated for very short decay lengths and one for long decay lengths. The remaining sampling distributions are identical for all samples and are listed in Table 2.4. The target number of events for each sample was  $2.5 \times 10^9$ .

**Table 2.4:** Generation level sampling distributions and ranges/values of the model dependent simulation samples.

Variable	Distribution	Range/Value
energy	$E^{-2}$	[2 GeV, $1 \times 10^4$ GeV]
zenith	uniform (in $\cos(\theta)$ )	[80°, 180°]
azimuth	uniform	[0°, 360°]
vertex $x, y$	uniform	$r=600$ m
vertex $z$	uniform	-600 m to 0 m
$m_4$	fixed	[0.3, 0.6, 1.0] GeV
$L_{\text{decay}}$	$L^{-1}$	[0.0004, 1000] m

### 2.2.3 Weighting Scheme

To produce physically correct event distributions based on the simplified generation sampling distributions for the HNL simulation, the forward folding method that was already introduced for the SM simulation in Section ?? is also used. The only required input is the mixing strength  $|U_{\tau 4}|^2$ , which is the variable physics parameter in this analysis. For each event the gamma factor

$$\gamma = \frac{\sqrt{E_{\text{kin}}^2 + m_4^2}}{m_4}, \quad (2.21)$$

is calculated, with the HNL mass  $m_4$ , and its kinetic energy  $E_{\text{kin}}$ . The speed of the HNL is calculated as

$$v = c \cdot \sqrt{1 - \frac{1}{\gamma^2}}, \quad (2.22)$$

where  $c$  is the speed of light. With these, the lab frame decay length range  $[s_{\min}, s_{\max}]$  can be converted into the rest frame lifetime range  $[\tau_{\min}, \tau_{\max}]$  for each event

$$\tau_{\min/\max} = \frac{s_{\min/\max}}{v \cdot \gamma}. \quad (2.23)$$

The proper lifetime of each HNL event can be calculated using the total decay width  $\Gamma_{\text{total}}$  from Section 1 and the chosen mixing strength  $|U_{\tau 4}|^2$  as

$$\tau_{\text{proper}} = \frac{\hbar}{\Gamma_{\text{total}}(m_4) \cdot |U_{\tau 4}|^2}, \quad (2.24)$$

where  $\hbar$  is the reduced Planck constant. Since the decay lengths or lifetimes of the events are sampled from an inverse distribution instead of an exponential, as it would be expected from a particle decay, we have to re-weight accordingly to achieve the correct decay lengths or lifetimes distribution. This is done by using the wanted exponential distribution

$$\text{PDF}_{\text{exp}} = \frac{1}{\tau_{\text{proper}}} \cdot e^{\frac{-\tau}{\tau_{\text{proper}}}}, \quad (2.25)$$

and the inverse distribution that was sampled from

$$\text{PDF}_{\text{inv}} = \frac{1}{\tau \cdot (\ln(\tau_{\max}) - \ln(\tau_{\min}))}. \quad (2.26)$$

This re-weighting factor is then calculated as

$$w_{\text{lifetime}} = \frac{\text{PDF}_{\text{exp}}}{\text{PDF}_{\text{inv}}} = \frac{\Gamma_{\text{total}}(m_4) \cdot |U_{\tau 4}|^2}{\hbar} \cdot \tau \cdot (\ln(\tau_{\max}) - \ln(\tau_{\min})) \cdot e^{\frac{-\tau}{\tau_{\text{proper}}}}. \quad (2.27)$$

Adding another factor of  $|U_{\tau 4}|^2$  to account for the mixing at the interaction vertex the total re-weighting factor becomes

$$w_{\text{total}} = |U_{\tau 4}|^2 \cdot w_{\text{lifetime}}. \quad (2.28)$$

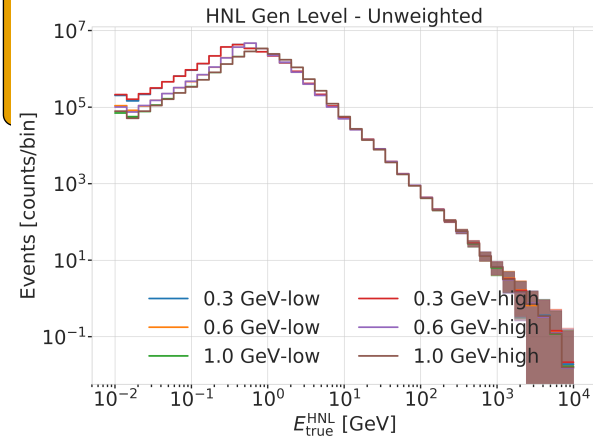
If this additional weighting factor is multiplied to a generation weight with units  $\text{m}^2$  (like in Equation ??), the livetime in  $\text{s}$ , and the oscillated primary neutrino flux in  $\text{m}^{-2}\text{s}^{-1}$ , it results in the number of expected events in the detector for this particular MC event for a chosen mixing (and mass).

JVS: The build-up of the weight expression is hard to follow without knowing where it's going. It may be better to start with the fact that the importance sampling weight is the ratio of PDFs, then write down each pdf, then drill down into each of the terms (basically, the standard "tell me what you're going to tell me, then tell me, then tell me what you told me" scheme). (RED)

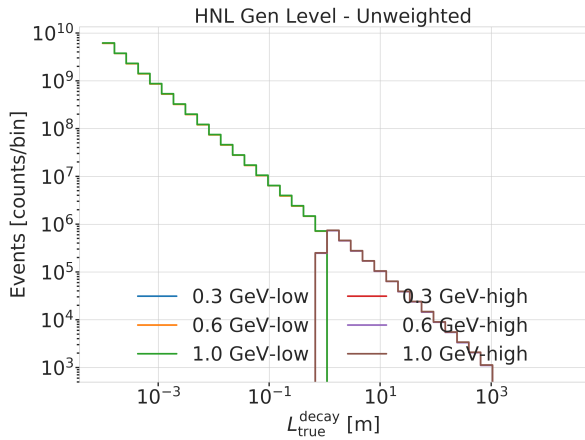
### 2.2.4 Generation Level Distributions

Figure 2.6 shows some selected generation level distributions. Additional distributions can be found in Figure ??.

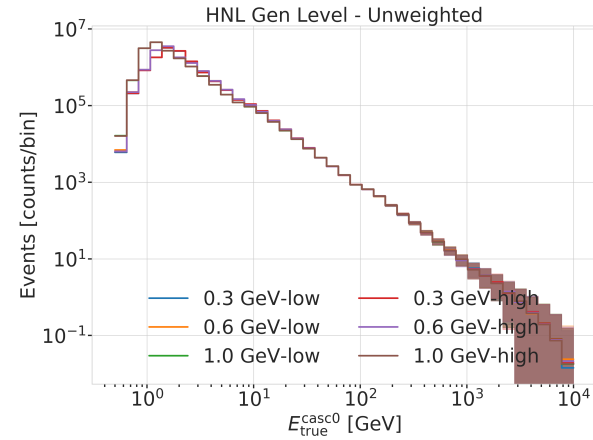
Combine low/high plots  
and remove all traces



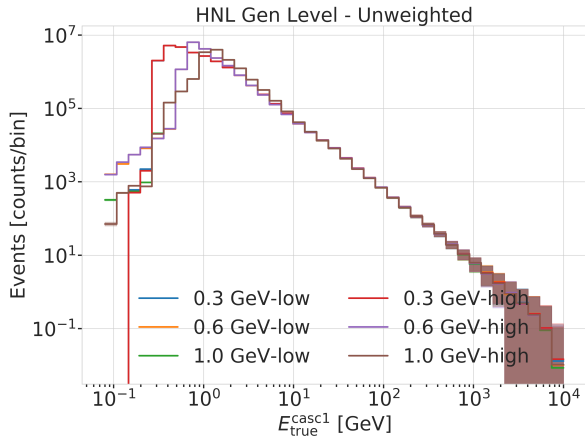
(a) HNL energy



(b) Decay length



(c) First cascade energy



(d) Second cascade energy

**Figure 2.6:** Generation level distributions of the model dependent simulation.

What is the message of these plots? Make it clear in the text and also in the captions. Potentially cut down to one or two and leave the rest or move them to the appendix. (RED)

# Detecting Low Energetic Double Cascades

# 3

## 3.1 Reconstruction

All existing reconstruction algorithms applied for low energetic atmospheric neutrino events mentioned in Section ?? are either assuming a single cascade hypothesis or a track and cascade hypothesis, which are the two SM morphologies observable at these energies, as was described in Section 1.3. A HNL being produced and decaying inside the IceCube detector however, will produce two cascade like light depositions. The morphology and how the cascade properties and their spatial separation depend on the model parameters was introduced in Section ?? To investigate the performance of the detector to observe these events, a low energetic double cascade reconstruction algorithm was developed, based on a pre-existing algorithm used to search for double cascades produced from high energetic astrophysical tau neutrinos [29] that was established in [30], but first mentioned in [31].

### 3.1.1 Table-Based Minimum Likelihood Algorithms

The reconstruction is relying on a maximum likelihood algorithm, which is the *classical* approach to IceCube event reconstructions, as opposed to ML based methods. A Poissonian likelihood is constructed, which compares the observed photon numbers,  $n$ , with their arrival times to the expected light depositions,  $\mu$ , for a given even hypothesis as

$$\ln(L) = \sum_j \sum_t n_{j,t} \cdot \ln(\mu_{j,t}(\Theta) + \rho_{j,t}) - (\mu_{j,t}(\Theta) + \rho_{j,t}) - \ln(n_{j,t}!) , \quad (3.1)$$

where  $\rho$  are the number of expected photons from noise,  $\Theta$  are the parameters governing the source hypothesis, and the likelihood is calculated summing over all DOMs  $j$  splitting observed photons into time bins  $t$ . The light expectations are calculated using look-up tables [24] that contain the results from MC simulations of reference cascade events or track segments. By varying the parameters defining the event hypothesis, the likelihood of describing the observed light pattern by the expected light depositions is maximized to find the reconstructed event. Algorithms of this kind used in IceCube are described in great detail in [5]. For the table production a specific choice of ice model has to be made, while the calibrated DOM information is taken from the measurement itself.

Based on the tabulated light expectations for cascades and track segments, various event hypothesis can be constructed, like the common cascade only or the track and cascade hypotheses. The hypothesis describing the double cascade signature of the HNL is using two reference cascades that are separated by a certain distance. The whole hypothesis is defined by 9 parameters and assumes that the two cascades are aligned with each other, which is a safe assumption for strongly forward boosted interactions. The parameters are the position of the first cascade  $x, y, z$ , the direction of both cascades  $\phi, \theta$ , and its time  $t$  as well as the decay length  $L$  between the

3.1	Reconstruction . . . . .	19
3.2	Double Cascade Classification . . . . .	26
3.3	Generic Double Cascade Performance . .	29

[29]: Abbasi et al. (2020), “Measurement of Astrophysical Tau Neutrinos in IceCube’s High-Energy Starting Events”

[30]: Usner (2018), “Search for Astrophysical Tau-Neutrinos in Six Years of High-Energy Starting Events in the IceCube Detector”

[31]: Hallen (2013), “On the Measurement of High-Energy Tau Neutrinos with IceCube”

maybe I want a figure for this, or not so important? (YELLOW)

[24]: Whitehorn et al. (2013), “Penalized splines for smooth representation of high-dimensional Monte Carlo datasets”

[5]: Aartsen et al. (2014), “Energy Reconstruction Methods in the IceCube Neutrino Telescope”

Elaborate whether this is the case (show it in a plot?). Discuss directionality of cascades in general. (ORANGE)

two cascades. Assuming the speed of the HNL to be the speed of light,  $c$ , this already defines the full signature. The HNL particle does not produce any light while traveling, as it is electrically neutral. The full 9 parameters describing the event are  $\Theta = (x, y, z, t, \theta, \phi, E_0, E_1, L)$ . To compute the full likelihood the term in Equation 3.1 is summed over both cascade parts,  $i$ , as  $\sum_i \ln(L_i)$ .

### 3.1.2 Optimization for Low Energy Events

Optimizing the double cascade reconstruction for low energetic events was done in parallel to the development of the model dependent simulation generator introduced in Section 2.2. A preliminary sample of HNL events was used, containing a continuum of masses between 0.1 GeV and 1.0 GeV and lab frame decay lengths sampled uniformly in the range from 5 m to 500 m. Even though this sample is not representative of a physically correct model and therefore not useful to predict the event expectation, it can still be used to optimize the reconstruction. The double cascade nature of the individual events and the evenly spaced decay length distribution are especially useful for this purpose.

[32]: Abbasi et al. (2022), “Low energy event reconstruction in IceCube DeepCore”

The simulation is processed up to Level 5 of the selection chain described in Section ?? and one of the reconstructions from [32] is applied to the events, fitting a cascade and a track and cascade hypothesis. The results from this reconstruction are used as an input for the double cascade reconstruction, where the position of the vertex, the direction of the event, and its interaction time are used as the input quantities for the first cascade, and the length of the track reconstruction is used as a seed for the distance between the two cascades.

#### Decay Length Seeds

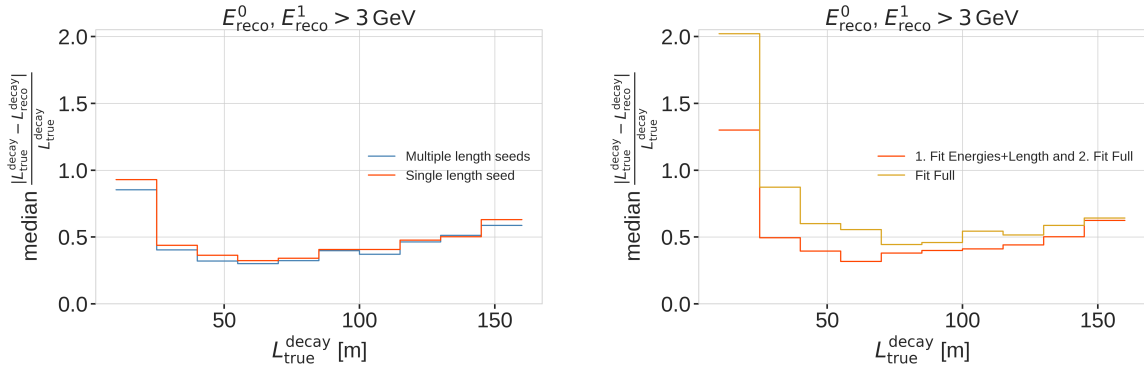


**Figure 3.1**  
fix caption of this figure  
(RED)

The full 9 dimensional likelihood space is very complex and can have many local minima, depending on the specific event and its location in the detector. Especially the seed value of the length between the two cascades was found to have a very strong impact on whether the global minimum was found during the minimization. To mitigate this effect, multiple fits are performed, seeding with variations of the input length at different orders of magnitude. The best result is used, selected based on the total likelihood value of the

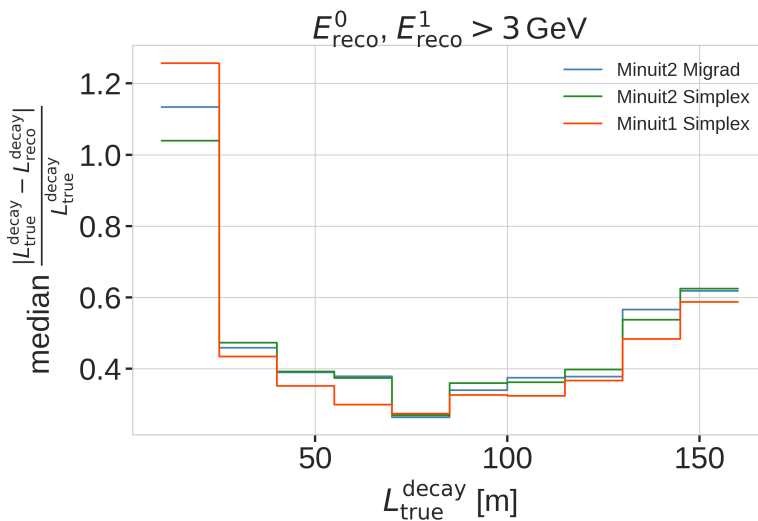
best fit parameter set. A small improvement in the decay length resolution can be found by using this approach as compared to a single length seed. The effect can be seen in the left part of Figure 3.1, which shows the median, absolute, fractional decay length resolution.

### Fit Routine

Because the length seed showed to have such a large impact on the reconstruction performance, a more sophisticated fit routine, than just fitting all 9 parameters at once, was tested. In a first fit iteration, some parameters are fixed and the resulting best fit point is used to fit all 9 parameters in a second iteration. In the right part of Figure 3.1 it can be seen how a fit split into two consecutive steps, where the first step fits only both cascade energies and the decay length and the second step fits the full 9 parameters, performs better as compared to a single, full 9 parameter fit. The initial seed for both routines is the same.

### Minimizer Settings

To investigate the effect of the minimizer used to find the best fit parameters, the reconstruction was performed using three different minimizers, which were easily accessible within the reconstruction framework. The minimizers used were Minuit1 Simplex, Minuit2 Simplex, and Minuit2 Migrad. The results can be seen in Figure 3.2, where the Minuit1 Simplex minimizer performs best. The initial idea was to test a global minimizer, or a routine that can find the rough position of the global minimum first and then a local minimizer to find the exact minimum, but unfortunately this was not possible with the minimizers available in the framework. From the three tested minimizers, Minuit1 Simplex performed best and was chosen as the default for the reconstruction. The comparison of the decay length resolutions can be seen in Figure 3.2.



fix caption of this figure  
(RED)

Figure 3.2: title

### 3.1.3 Performance

The chosen reconstruction chain used to test the performance of the detector to observe low energetic double cascades is the following; Minuit1 Simplex is used as the minimizer, the decay length is seeded with 3 different values, 0.5x, 1.0x, and 1.5x the length of the track reconstruction, and the fit routine is split into two steps, where the first step fits the energies and the decay length and the second step fits the full 9 parameters. In the first step, the number of time bins in Equation 3.1 is set to 1, so just the number of photons and their spatial information is used. The second step is seeded with the best results from the first fit and here the number of time bins is chosen such that each photon falls into a separate time bin, which means all time information is used. The average runtime per event is  $\sim 16$  s on a single CPU core, but is very dependent on the number of photons observed in the event, since the likelihood calculation in the second step scales with this number and a table lookup has to be performed for each photon.

To get a more realistic estimate of the reconstruction performance, it is run on a second preliminary sample of HNL events, containing masses between 0.1 GeV and 3.0 GeV and the lab frame decay length is sampled from an inverse distribution in the range from 1 m to 1000 m, which is a better approximation of the expected exponential decay distribution of the HNL. The performance is shown for events where the reconstruction chain was successfully run, the event selection criteria up to level 7 are fulfilled, and the reconstructed energy of both cascades is above 3.0 GeV. This is done to only investigate well reconstructed events with two significant light depositions at a usual final selection level of the oscillation analyses.

one half sentence on why  
this number was chosen?  
(ORANGE)

### Energy Resolutions

The energy resolution is inspected by looking at the 2-dimensional distribution of reconstructed energy versus the true energy as shown in Figure 3.3. The bin entries are shown as well as the median and  $\pm 25\%$  calculated per vertical column, to get an idea of the distribution for a given energy slice. The color scale is showing the PDF along in each true energy slice, which is the full information combined into the median $\pm 25\%$  lines. The reconstructed energy is only the energy that is observable from photons, while the true energy is the total cascade energy, including the parts that go into EM neutral particles that do not produce light. It is therefore not expected that the median lines up with the axis diagonal, but rather the reconstructed energy is going to be lower.

The histogram for the first cascade energy is shown on the left and above an energy of  $\sim 10$  GeV the reconstruction performs well, with the median being parallel to the diagonal and the spread in the  $\pm 25\%$  quantile being small. Below this energy the reconstruction is over-estimating the true energy, which is a known effect in IceCube, where the reconstruction is biased towards higher energies around the energy detection threshold, because events that enter the sample are events with an over fluctuation in their light deposition, which makes them pass into the selection and being reconstructible in the first place.

For the second cascade the overall behavior is similar, only that the energy where the reconstruction starts to perform good is higher around  $\sim 20$  GeV.

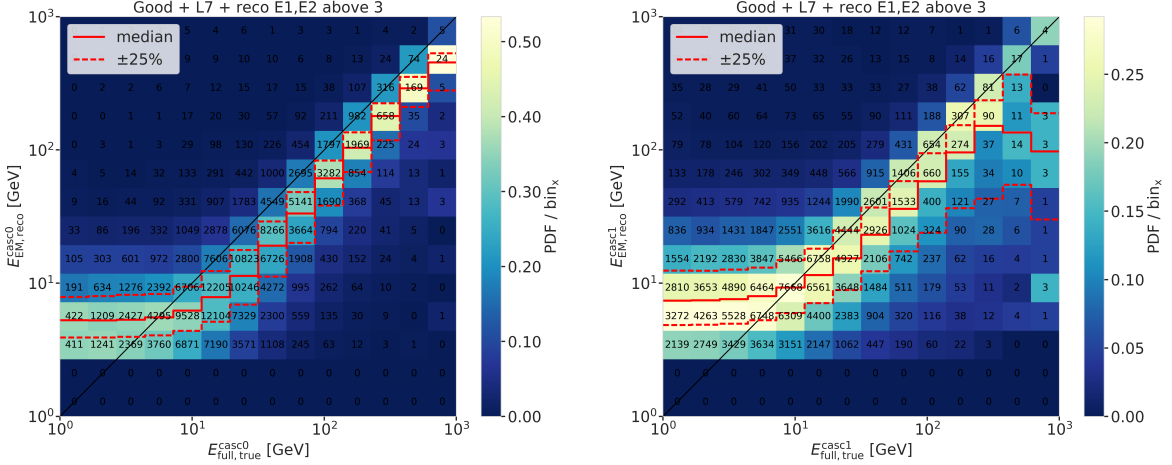


**Figure 3.3:** Reconstructed (EM) energy versus true energy (full) energy for the first cascade (left) and second cascade (right). The color scale is according to the PDF in each vertical true energy slice, with the solid and dashed lines showing the median $\pm 25\%$  quantiles. The bin entries are shown as numbers.

The spread around the median is also larger and starts to expand a lot above 200 GeV, where the statistics are lower as can be seen from the bin counts. It is also very apparent that the majority of energies of the second cascade are at lower true energy values between 1 GeV and 20 GeV.

For both cascade resolutions the effect of the reconstruction being biased towards lower values, due to the comparison of the full true energy to the reconstructed EM energy can be seen.

### Length Resolutions

The decay length resolution is also investigated by looking at a similar style of 2-d histograms as for the energies, where the reconstructed decay length is plotted versus the true decay length. The left part of Figure 3.4 shows the distributions after the same selection criteria from Section 3.1.3 are applied. It can be observed that for short true lengths the reconstruction is over-estimating the length, while for long true lengths the reconstruction is strongly under-estimating the length. There is a region between true lengths of 20 m and 80 m where the median reconstruction is almost unbiased, but the 50 % interquartile range is large and increasing from  $\sim 50$  m to  $\sim 70$  m with true decay lengths.

The over-estimation at small true lengths can be explained for multiple reasons, one being that the shortest DOM spacing is  $\sim 7$  m, vertically for DeepCore strings, but mostly larger than that, so resolving lengths below this is very complicated, and the reconstruction tends to be biased towards estimating the length around where the light was observed. Another reason is a similar argument to why the energies are over-estimated at small true values, namely that events that passed the selection and were reconstructed in those cases, probably have an over fluctuation in light deposition, extending further out from the vertices, so the reconstructed length is larger. Additionally, approaching a length of 0.0, the reconstructed length will of course always be a one-sided distribution, because the lengths have to be positive.

The under-estimation at large true lengths is more puzzling, and it seems like the distribution becomes bimodal in the reconstructed lengths, with

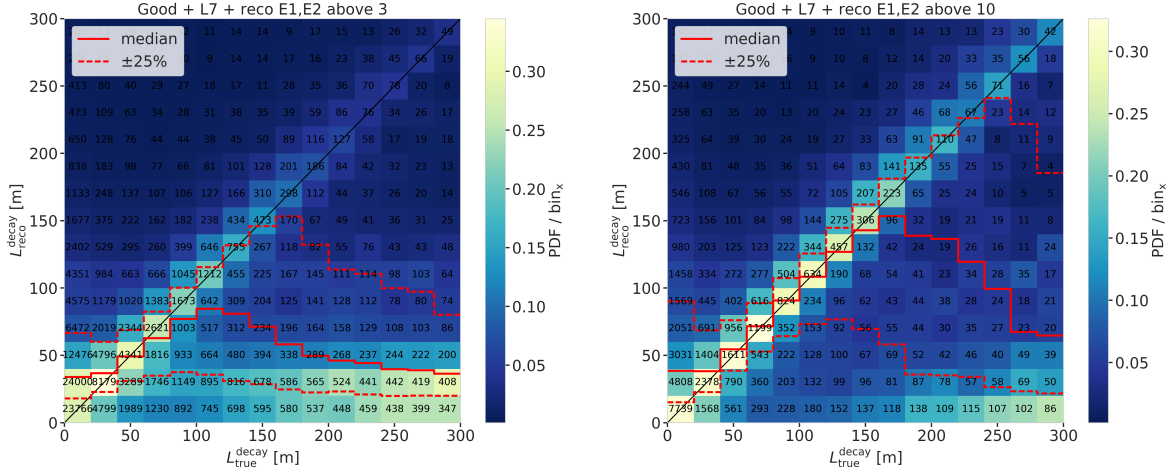


**Figure 3.4:** Reconstructed decay length versus true decay length for  $\sim 3$  GeV (left) and  $\sim 10$  GeV (right) minimum reconstructed cascade energies. The color scale is according to the PDF in each vertical true length slice, with the solid and dashed lines showing the median  $\pm 25\%$  quantiles. The bin entries are shown as numbers.

one population around the diagonal, meaning that they are properly reconstructed, and one population at very short reconstructed lengths, which are badly reconstructed. Above 150 m the badly reconstructed population starts to dominate, and the median resolution drops off strongly. The assumption is that for these events, only one cascade was observed with enough light to be reconstructed, and the reconstruction describes the one observed cascade in two parts, separated by a short distance, driven by similar factors as mentioned before. A quick check to confirm whether this is the case, was to increase the selection criteria to minimum reconstructed cascade energies of 10 GeV, which is shown in the right part of Figure 3.4. It can be seen that the median resolution is already much better, aligning with the expectation between 40 m and 160 m. Judging from the median resolution and the  $+25\%$  quantile in this range, there is very few events with an over-expectation in the energy, since both of them are alidgning with the diagonal. The spread towards lower reconstructed lengths, on the other hand, is still very large and above 200 m the badly reconstructed population starts to dominate again.

make on figure, where  
the two selected regions  
are highlighted? (RED)

fix caption (RED)

#### Badly Reconstructed Cascade Population

To investigate the badly reconstructed population further, a rough separation was made to find out what the cause of the difference is. It was already established that a larger reconstructed energy in both cascades, which is related to a larger true energy in form of more deposited light, leads to a better reconstruction in more events. As shown in Figure 3.5, only events with true decay length larger than 80 m are used, where the populations are split by the reconstructed decay length being larger or smaller than 80 m. Based on a few potential sourced of bad reconstruction, several variables were checked to see if there is a difference between the two populations.

The left part of Figure 3.6 shows the true horizontal distance of the second cascade from string 36. The distance is denoted as  $\rho_{36}$  and is a very good proxy for the distance to the center of the detector, because string 36 is almost at the center. While the distributions looks very similar for the first cascade

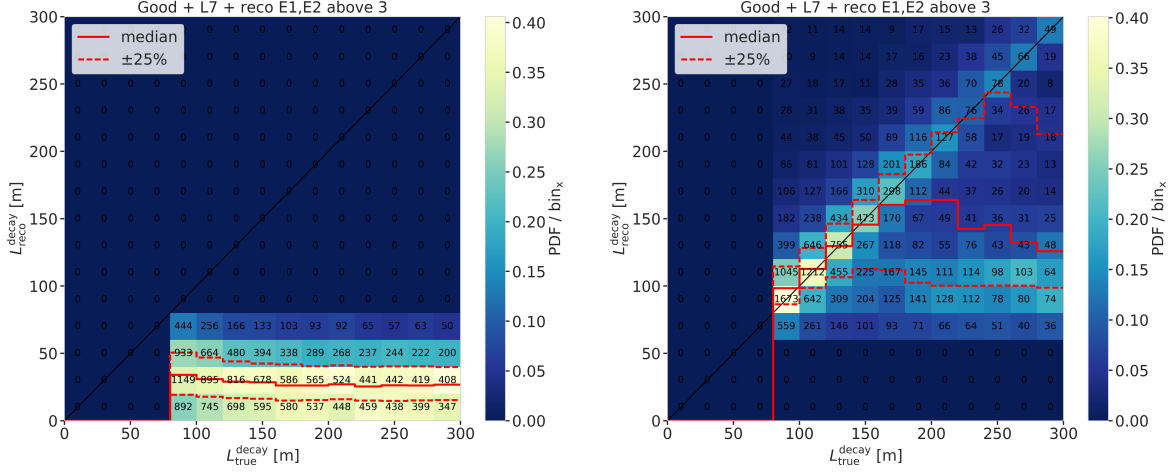


**Figure 3.5**

(not shown), for the second cascade the badly reconstructed population extends to larger values. Considering that the DeepCore strings are roughly inside a 70 m radius from the center, and the next layer of IceCube strings is at a radius of 125 m, this is a plausible explanation for a worse reconstruction, because for the badly reconstructed population the second cascades are more often in regions without DOMs, so less or no light is observed from them.

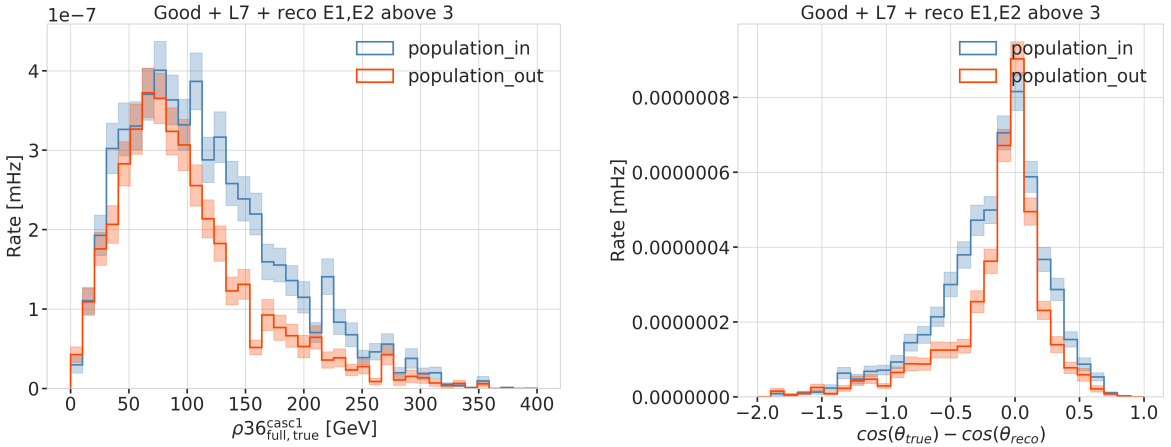


**Figure 3.6**

Another possible reason why the reconstruction underperforms could be that the initial seed direction was off and therefore one of the cascades cannot be found properly. Looking at the error of the cosine of the reconstructed zenith angle shown in the right of Figure 3.6, we see that the badly reconstructed population has a larger error, and is less peaked around 0.0. This could be a hint that the direction is worse for the badly reconstructed population, which could be due to a bad seed direction, or just the result of one cascade not being observed properly.

The true energies of both cascades are shown in Figure 3.5, where it can be observed that the first cascade energy is generally much larger than the second, peaking between 10 GeV and 20 GeV, while the second cascade peaks

re-make normalized?  
(ORANGE)

fix caption (RED)

re-make normalized?  
(ORANGE)

fix caption (RED)

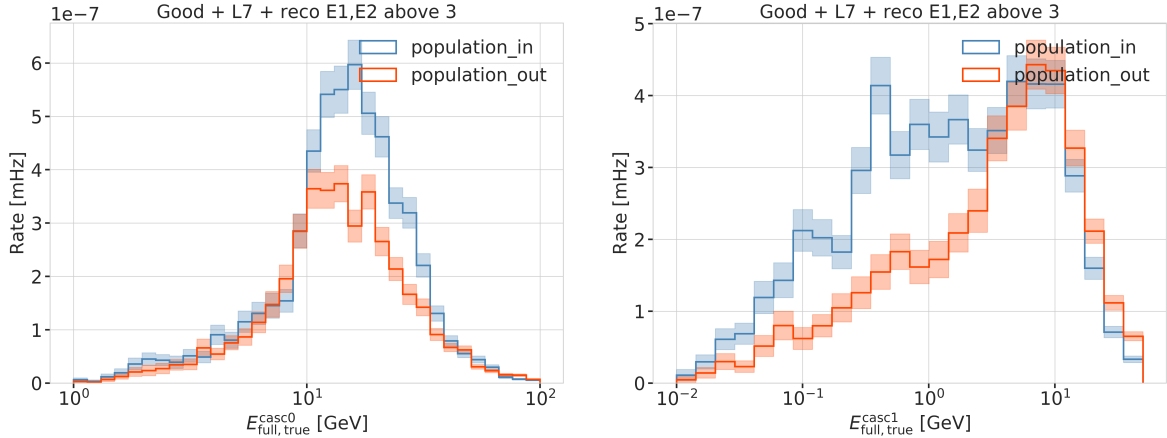


Figure 3.7

below 10 GeV. For the first cascade there is no significant difference between the two populations, but for the second cascade the badly reconstructed population has a larger fraction of events with lower energies and the distribution is almost uniform in the range of 2 GeV to 10 GeV, while the well reconstructed population has a peak around 10 GeV and falls off faster towards lower energies. This is a strong indication that the main reason for the bad reconstruction is the low energy of the second cascade.

Despite the fact that the split into the two populations was very rudimentary, it is clear that the main reason for the bad reconstruction is the low energy of the second cascade, while other factors, like the position of the second cascade, or the potentially bad input seed direction are also contributing to the bad reconstruction. For a more thorough investigation, a more sophisticated separation would be needed, but this is sufficient to conclude that the main reason for the bad reconstruction is the low energy of the second cascade.

circle back to the energy distributions I showed somewhere else, and state how the cascade energies are distributed in general (ORANGE)

fix caption (RED)

## 3.2 Double Cascade Classification

Even though the performance results show that it is very complicated to reconstruct these low energetic double cascade events, the attempt to identify them in the background of SM neutrino events was made. For this purpose a classifier was trained to distinguish between HNL *signal* events and SM neutrino *background* events, using the same preliminary sample of HNL events as was used to assess the reconstruction performance. To mitigate the effect of the bad reconstruction, a set of cuts was applied to make sure the classifier is trained on well reconstructed events, which were chosen as events with a minimum reconstructed energy of both cascades of 5 GeV and a minimum reconstructed decay length of 40 m. These cuts were applied to both signal and background events.

Additionally, some cuts on the true energies and decay length were applied for the signal, which are a minimum true energy of both cascades of 5 GeV, and a true decay length between 40 m and 150 m. These were chosen to make sure the HNL events were theoretically double cascade like and at a sensible length scale inside DeepCore. Figure 3.8 shows the decay length 2-d histograms after the cuts were applied.

add table with cuts?  
(YELLOW)

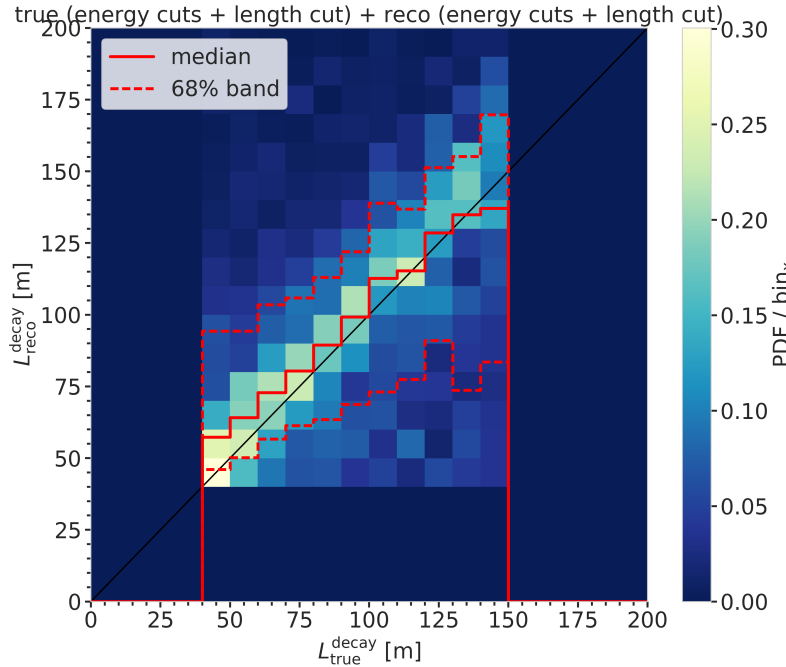


Figure 3.8

The classifier used was a *Boosted Decision Tree (BDT)* from the *scikit-learn* package [33] and the input features are taken from the double cascade reconstruction explained in Section 3.1 as well as some additional variables from earlier levels of the processing explained in Section ??.

Both a single classifier trained to distinguish between HNL signal events and all SM background events was tested as well as two classifiers, one trained to distinguish signal from track like background and the other signal from cascade like background separately. Since the SM neutrino events at these energies are either track like or cascade like, the latter approach was expected to perform better.

[33]: Pedregosa et al. (2011), “Scikit-learn: Machine Learning in Python”

add example features?  
maybe like 2 or so? decay  
length and one other?  
(RED)

fix caption of this figure  
(RED)

### 3.2.1 Classification Results

Despite the fact that several combinations of features and classifier hyperparameters were tested, it was not possible to identify a pure double cascade region with a single classifier. Figure 3.10 shows the output probability of the classifier trained to distinguish double cascade like signals from track like background, applied to the full data sample containing all signal and background events. A probability of 1 means very signal like, and only the region close to 1 is shown to highlight that there is always signal and background events in every bin.

fix caption (RED)

Applying the two classifiers trained to distinguish signal from track and signal from cascade, it is possible to select a region with only signal events. This is visualized in Figure 3.11, but when applying a weight to the signal events selected by applying two cuts on the probabilities, the rate of the selected signal events is very low. Assuming a very optimistic mixing of 1 it would take more than 20 years of data taking to observe a single event and with this low simulation statistics the prediction is not very reliable.

Make a single plot, showing S/B or so? (RED)

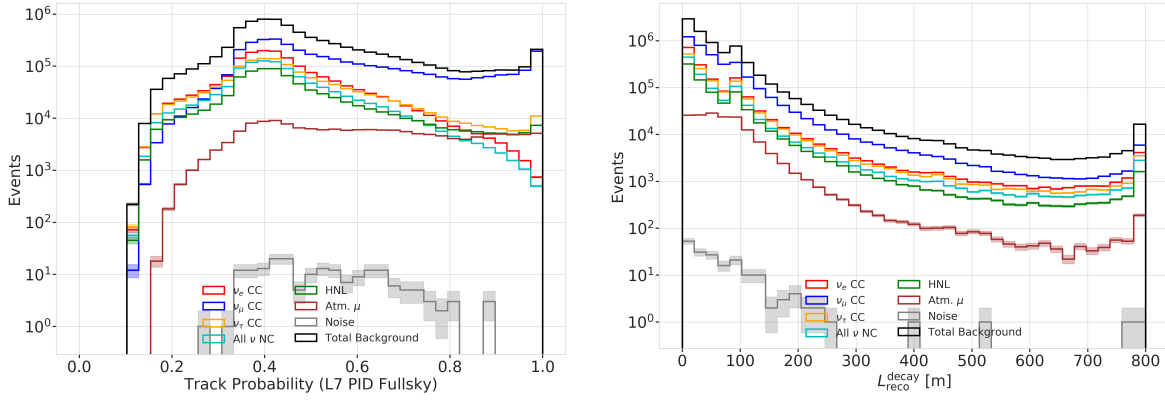


Figure 3.9

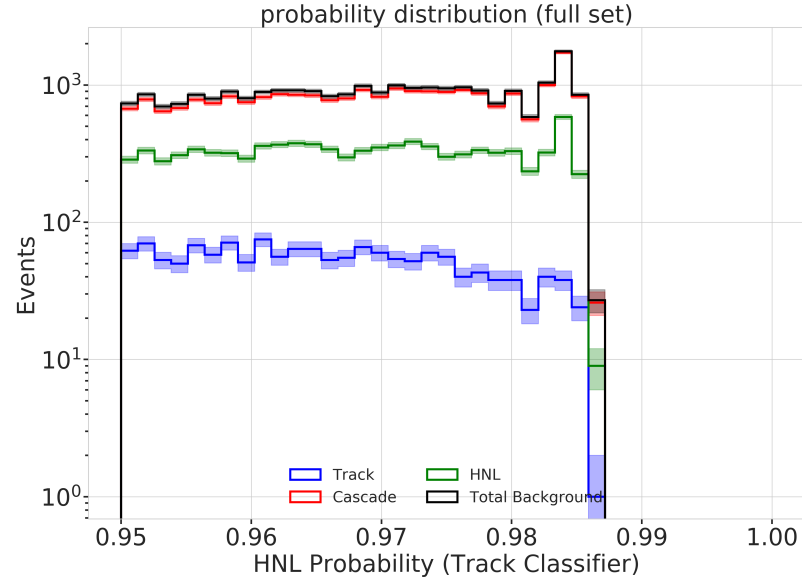


Figure 3.10

Making a weaker cut to select a signal like region will contain a large amount of background events, which dominate over the signal at  $\sim 2$  orders of magnitude for a mixing of 0.1. The conclusion from this is, that with the current selection and reconstruction chain and a classical BDT, it is not possible to distinguish signal events at a level feasible to perform an analysis

fix caption of this figure  
(RED)

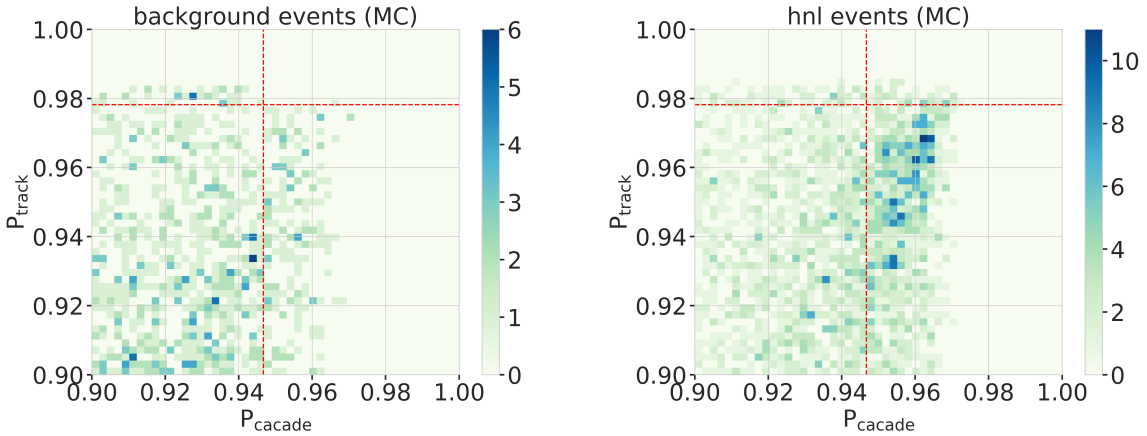


Figure 3.11

### 3.3 Generic Double Cascade Performance

All the above results were obtained using a preliminary version of the model dependent HNL simulation. To investigate the effect of the low energy event selection and the double cascade reconstruction performance in a more generic way, the model independent simulation introduced in Section 2.1 was used to perform the same tests and a series of additional checks. The important advantage is the controllable parameter space, especially in cascade energies and decay length, because the event kinematics are not coupled to the underlying HNL model, but can be chosen freely. This means that some benchmark edge cases can be investigated, and the performance can also be assessed for a realistic scenario in addition to mapping out the effects of the event selection and where the reconstruction breaks down.

describe the "good fit" selection when I first show plots that use it (ORANGE)

#### 3.3.1 Idealistic Events

The *best case* scenario to observe an event is to be directly on top of a string with a straight up-going direction. Using the simulation sample introduced in Section 2.1.1 and running the double cascade reconstruction from Section 3.1 on the events, it is possible to estimate the performance limit of the reconstruction. Figure 3.12 shows one example event view from that sample, where the cascade energies are 2.4 GeV and 4.9 GeV, and the decay length is 20 m. It can be seen that despite the low energies, both cascades deposit light in the DOMs and the reconstruction is expected to work.

The performance of the length reconstruction is shown in Figure 3.13, where the median of the absolute, fractional decay length resolution is shown on the left and the 2-d histogram of the reconstructed versus the true decay length is shown on the right. The length is very well reconstructed, with the median resolution being below 30 % above a true decay length of  $\sim 10$  m, and falling off with increasing true length, down to  $\sim 10\%$  at 100 m.

The 2-d histogram shows that there is no under-estimation of the length up to a true decay length of  $\sim 210$  m, which shows that if there are DOMs in the region between the two cascades that have not observed any light, the reconstruction is very stable. Considering the underlying Poisson likelihood

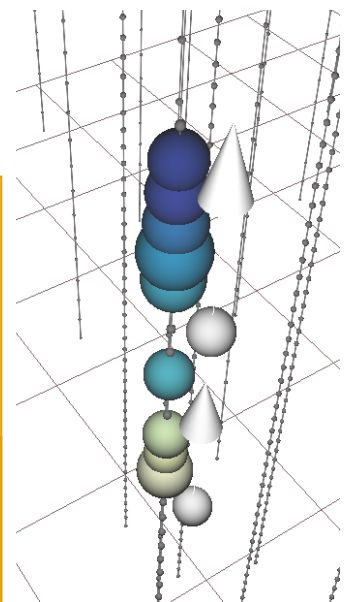


Figure 3.12

fix caption (RED)

Check this number (RED)

fix caption of this figure (RED)

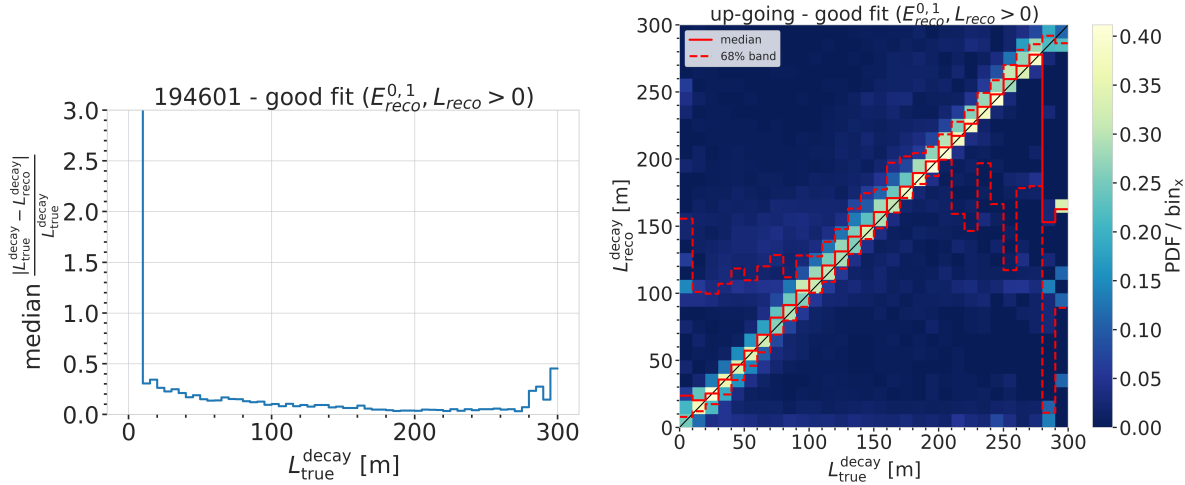


Figure 3.13

in Equation 3.1 used for the reconstruction, this makes sense, since DOMs being present, but not observing any light is affecting the light expectation that goes into the likelihood and therefore makes these hypotheses unlikely and therefore incompatible with the data.

### 3.3.2 Realistic Events

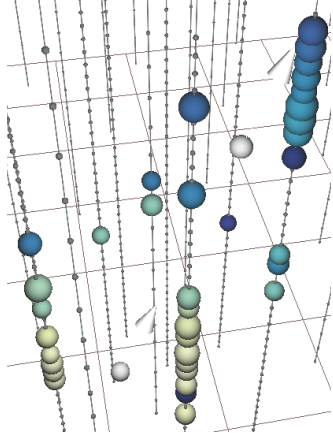


Figure 3.14

The sample of HNL events introduced in Section 2.1.2, which is a more realistic representation of the expected HNL events, but still offers more controlled energy and length distributions, is used to investigate the selection efficiency, to cross check the reconstruction performance, and to benchmark the limits where the reconstruction breaks down. An example event view is shown in Figure 3.14, for cascade energies of 30.8 GeV and 25.3 GeV, and a decay length of 100 m. Here it can be seen that even for these higher energies, if the cascades are further away from the strings, only individual photons are observed in the DOMs, and detecting and reconstructing them gets significantly more challenging.

### 3.3.3 Selection Efficiency

To assess the efficiency of the low energy event selection introduced in Section ??, the energy and length distributions are shown across the different selection levels in Figure ???. Table ?? shows the total efficiency of the selection, where it can be seen that at level xx it is reduced the most and only xx% of the events pass the selection to level 5.

### 3.3.4 Performance

#### 2-Dimensional Distributions

Looking at the energy distributions in Figure 3.15 shows a similar behavior to results discussed in Section 3.1.3, but here there is no bias in the reconstructed energy, because the events are simulated as EM cascades, which means all energy is deposited in light and can be reconstructed. Above around 5 GeV

fix caption (RED)

Check this number (RED)

Make/add relevant plots here (RED)

Plot energy (true total) and true decay length across the different levels (RED)

Make table with the rates across the different levels for benchmark mass/mixing (RED)

to 6 GeV the median is very stable, and the 1-sigma resolution band is 50 % narrow and decreasing with energy down to 20 % at 100 GeV. Interestingly, the second cascade energy reconstruction performs slightly worse, although they have the same energy ranges for this sample. This could hint at an asymmetry in the reconstruction process, which might relate to how the two cascades are parameterized, or be due to the different positions and the dominantly up-going direction used in the sampling combined with the DOMs looking down. The total energy resolution shown in the left part of Figure 3.16 is very good, above 10 GeV it is unbiased and the 1-sigma resolution band is below 20 %.

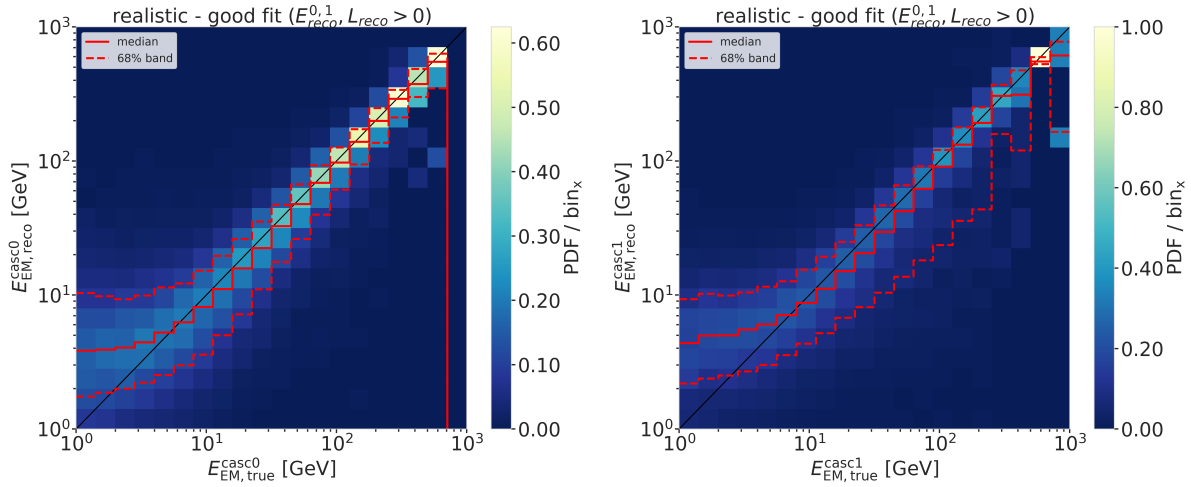


**Figure 3.15**

fix caption of this figure  
(RED)

The decay length resolution shown in the right part of Figure 3.16 looks similarly bad to the results discussed in Section 3.1.3 and shows the same features with a region between 20 m and 80 m where it is roughly unbiased, but the 1-sigma resolution band is wide with a lot of outliers towards short reconstructed lengths. Below 20 m the reconstructed lengths are always over-estimating the true and above 80 m a population of events start to dominate where the decay lengths is not getting reconstructed at all, as investigated before.

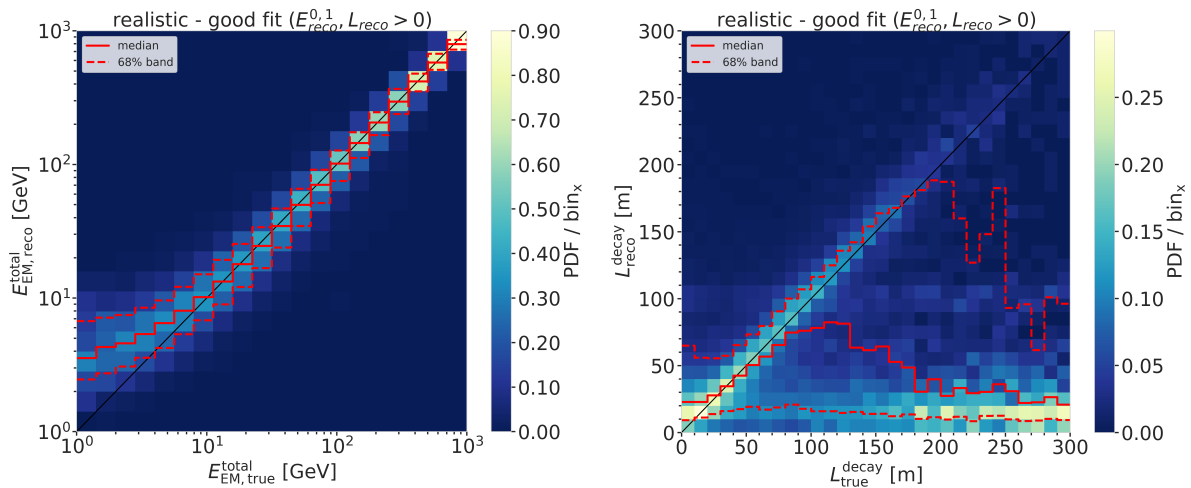


**Figure 3.16**

fix caption of this figure  
(RED)

**Decay Length Resolution** As already mentioned before, the decay length resolution is much worse than the energy resolutions. Figure 3.17 also shows that the median is below 0.0 for short true length and above 0.0 and approaching 1.0 for long true lengths.

To investigate whether this is really due to the fact that one of the cascades is not observed, the decay length resolution was plotted against the total energy of the event and the minimum energy of the two cascades Figure 3.18.

It can be seen that the median of the decay length resolution stabilizes at 0.0 for a total energy above 20 GeV, but the spread of the distribution is still quite large with a 1-sigma band of 80 % to 100 %.

From the plot against the minimum energy it can be seen that the decay length resolution starts to be unbiased for a minimum energy of the cascades of 7 GeV, with an equivalently large spread.

A preliminary takeaway from this is that the decay length reconstruction is not reliable at all for events with a total energy below 20 GeV or a minimum cascade energy below 7 GeV.

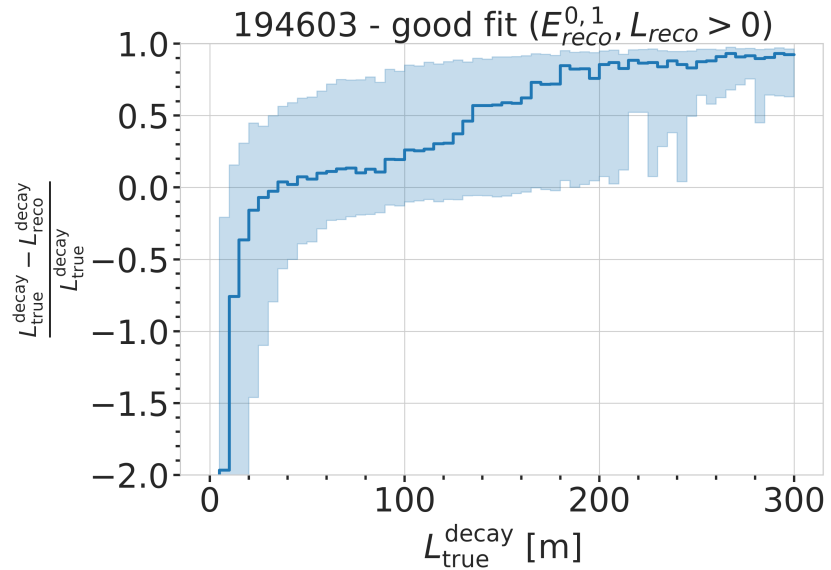


Figure 3.17  
fix caption of this figure  
(RED)

fix caption of this figure  
(RED)

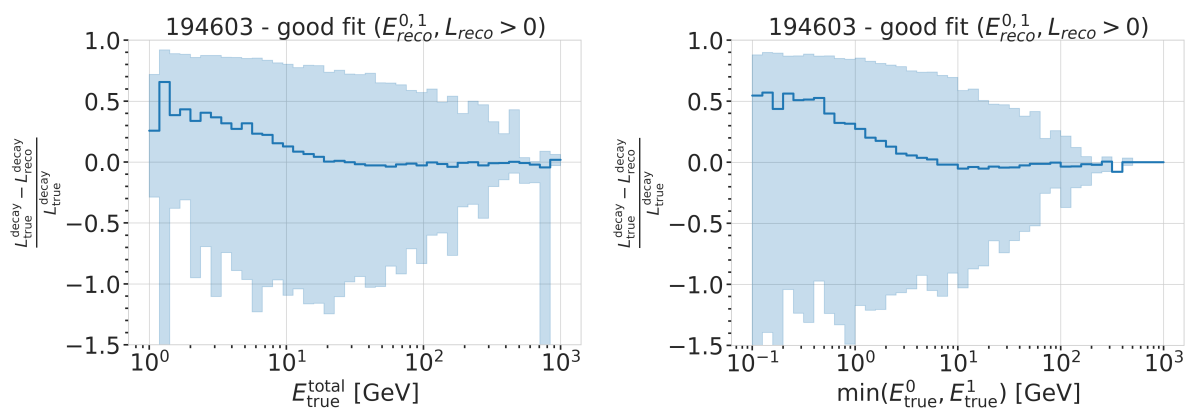


Figure 3.18



# Bibliography

Here are the references in citation order.

- [1] M. G. Aartsen et al. "The IceCube Neutrino Observatory: instrumentation and online systems". In: *Journal of Instrumentation* 12.3 (Mar. 2017), P03012. doi: [10.1088/1748-0221/12/03/P03012](https://doi.org/10.1088/1748-0221/12/03/P03012) (cited on pages 1, 3).
- [2] P. B. Price, K. Woschnagg, and D. Chirkin. "Age vs depth of glacial ice at South Pole". In: *Geophysical Research Letters* 27.14 (2000), pp. 2129–2132. doi: <https://doi.org/10.1029/2000GL011351> (cited on page 2).
- [3] R. Abbasi et al. "In-situ estimation of ice crystal properties at the South Pole using LED calibration data from the IceCube Neutrino Observatory". In: *The Cryosphere Discussions* 2022 (2022), pp. 1–48. doi: [10.5194/tc-2022-174](https://doi.org/10.5194/tc-2022-174) (cited on page 2).
- [4] R. Abbasi et al. "The IceCube data acquisition system: Signal capture, digitization, and timestamping". In: *Nuclear Instruments and Methods in Physics Research Section A: Accelerators, Spectrometers, Detectors and Associated Equipment* 601.3 (2009), pp. 294–316. doi: <https://doi.org/10.1016/j.nima.2009.01.001> (cited on pages 2, 3).
- [5] M. G. Aartsen et al. "Energy Reconstruction Methods in the IceCube Neutrino Telescope". In: *JINST* 9 (2014), P03009. doi: [10.1088/1748-0221/9/03/P03009](https://doi.org/10.1088/1748-0221/9/03/P03009) (cited on pages 3, 19).
- [6] J. Feintzeig. "Searches for Point-like Sources of Astrophysical Neutrinos with the IceCube Neutrino Observatory". PhD thesis. University of Wisconsin, Madison, Jan. 2014 (cited on page 3).
- [7] N. Kulacz. "In Situ Measurement of the IceCube DOM Efficiency Factor Using Atmospheric Minimum Ionizing Muons". MA thesis. University of Alberta, 2019 (cited on page 3).
- [8] R. Abbasi et al. "The design and performance of IceCube DeepCore". In: *Astropart. Phys.* 35.10 (2012), pp. 615–624. doi: [10.1016/j.astropartphys.2012.01.004](https://doi.org/10.1016/j.astropartphys.2012.01.004) (cited on page 3).
- [9] P. A. Cherenkov. "Visible Radiation Produced by Electrons Moving in a Medium with Velocities Exceeding that of Light". In: *Phys. Rev.* 52 (4 Aug. 1937), pp. 378–379. doi: [10.1103/PhysRev.52.378](https://doi.org/10.1103/PhysRev.52.378) (cited on page 4).
- [10] I. Frank and I. Tamm. "Coherent visible radiation from fast electrons passing through matter". In: *C. R. Acad. Sci. USSR* 14 (1937), pp. 109–114 (cited on pages 4, 5).
- [11] I. Tamm. "Radiation Emitted by Uniformly Moving Electrons". In: *Selected Papers*. Ed. by B. M. Bolotovskii, V. Y. Frenkel, and R. Peierls. Berlin, Heidelberg: Springer Berlin Heidelberg, 1991, pp. 37–53. doi: [10.1007/978-3-642-74626-0\\_3](https://doi.org/10.1007/978-3-642-74626-0_3) (cited on pages 4, 5).
- [12] L. Rädel and C. Wiebusch. "Calculation of the Cherenkov light yield from low energetic secondary particles accompanying high-energy muons in ice and water with Geant4 simulations". In: *Astroparticle Physics* 38 (Oct. 2012), pp. 53–67. doi: [10.1016/j.astropartphys.2012.09.008](https://doi.org/10.1016/j.astropartphys.2012.09.008) (cited on page 5).
- [13] D. Chirkin and W. Rhode. "Propagating leptons through matter with Muon Monte Carlo (MMC)". In: (July 2004) (cited on pages 5, 6).
- [14] L. Raedel. "Simulation Studies of the Cherenkov Light Yield from Relativistic Particles in High-Energy Neutrino Telescopes with Geant4". MA thesis. Aachen, Germany: Rheinisch-Westfälischen Technischen Hochschule, 2012 (cited on pages 5, 6).
- [15] M. Tanabashi et al. "Review of Particle Physics". In: *Phys. Rev. D* 98 (3 Aug. 2018), p. 030001. doi: [10.1103/PhysRevD.98.030001](https://doi.org/10.1103/PhysRevD.98.030001) (cited on page 6).
- [16] S. Agostinelli et al. "Geant4—a simulation toolkit". In: *Nucl. Instr. Meth. Phys. Res.* 506.3 (July 2003), pp. 250–303. doi: [10.1016/s0168-9002\(03\)01368-8](https://doi.org/10.1016/s0168-9002(03)01368-8) (cited on page 6).

- [17] T. Gabriel et al. "Energy dependence of hadronic activity". In: *Nuclear Instruments and Methods in Physics Research Section A: Accelerators, Spectrometers, Detectors and Associated Equipment* 338.2 (1994), pp. 336–347. doi: [https://doi.org/10.1016/0168-9002\(94\)91317-X](https://doi.org/10.1016/0168-9002(94)91317-X) (cited on page 6).
- [18] A. Terliuk. "Measurement of atmospheric neutrino oscillations and search for sterile neutrino mixing with IceCube DeepCore". PhD thesis. Berlin, Germany: Humboldt-Universität zu Berlin, Mathematisch-Naturwissenschaftliche Fakultät, 2018. doi: [10.18452/19304](https://doi.org/10.18452/19304) (cited on page 7).
- [19] L. Fischer. [https://github.com/LeanderFischer/icetray\\_double\\_cascade\\_generator\\_functions](https://github.com/LeanderFischer/icetray_double_cascade_generator_functions) (cited on page 9).
- [20] R. Abbasi et al. "LeptonInjector and LeptonWeighter: A neutrino event generator and weighter for neutrino observatories". In: *Comput. Phys. Commun.* 266 (2021), p. 108018. doi: [10.1016/j.cpc.2021.108018](https://doi.org/10.1016/j.cpc.2021.108018) (cited on page 12).
- [21] P. Coloma et al. "GeV-scale neutrinos: interactions with mesons and DUNE sensitivity". In: *Eur. Phys. J. C* 81.1 (2021), p. 78. doi: [10.1140/epjc/s10052-021-08861-y](https://doi.org/10.1140/epjc/s10052-021-08861-y) (cited on pages 13, 15, 16).
- [22] J. Alwall et al. "The automated computation of tree-level and next-to-leading order differential cross sections, and their matching to parton shower simulations". In: *JHEP* 07 (2014), p. 079. doi: [10.1007/JHEP07\(2014\)079](https://doi.org/10.1007/JHEP07(2014)079) (cited on page 13).
- [23] C. Argüelles. <https://github.com/arguelles/NuXSSplMkr> (cited on pages 13, 14).
- [24] N. Whitehorn, J. van Santen, and S. Lafebre. "Penalized splines for smooth representation of high-dimensional Monte Carlo datasets". In: *Computer Physics Communications* 184.9 (2013), pp. 2214–2220. doi: <https://doi.org/10.1016/j.cpc.2013.04.008> (cited on pages 13, 19).
- [25] J.-M. Levy. "Cross-section and polarization of neutrino-produced tau's made simple". In: *J. Phys. G* 36 (2009), p. 055002. doi: [10.1088/0954-3899/36/5/055002](https://doi.org/10.1088/0954-3899/36/5/055002) (cited on page 14).
- [26] E. Tiesinga et al. "CODATA recommended values of the fundamental physical constants: 2018". In: *Rev. Mod. Phys.* 93 (2 July 2021), p. 025010. doi: [10.1103/RevModPhys.93.025010](https://doi.org/10.1103/RevModPhys.93.025010) (cited on page 15).
- [27] <https://launchpad.net/mg5amcnlo/3.0/3.3.x> (cited on page 16).
- [28] A. Alloul et al. "FeynRules 2.0 - A complete toolbox for tree-level phenomenology". In: *Comput. Phys. Commun.* 185 (2014), pp. 2250–2300. doi: [10.1016/j.cpc.2014.04.012](https://doi.org/10.1016/j.cpc.2014.04.012) (cited on page 16).
- [29] R. Abbasi et al. "Measurement of Astrophysical Tau Neutrinos in IceCube's High-Energy Starting Events". In: *arXiv e-prints* (Nov. 2020) (cited on page 19).
- [30] M. Usner. "Search for Astrophysical Tau-Neutrinos in Six Years of High-Energy Starting Events in the IceCube Detector". PhD thesis. Berlin, Germany: Humboldt-Universität zu Berlin, Mathematisch-Naturwissenschaftliche Fakultät, 2018. doi: [10.18452/19458](https://doi.org/10.18452/19458) (cited on page 19).
- [31] P. Hallen. "On the Measurement of High-Energy Tau Neutrinos with IceCube". MA thesis. Aachen, Germany: RWTH Aachen University, 2013 (cited on page 19).
- [32] R. Abbasi et al. "Low energy event reconstruction in IceCube DeepCore". In: *Eur. Phys. J. C* 82.9 (2022), p. 807. doi: [10.1140/epjc/s10052-022-10721-2](https://doi.org/10.1140/epjc/s10052-022-10721-2) (cited on page 20).
- [33] F. Pedregosa et al. "Scikit-learn: Machine Learning in Python". In: *Journal of Machine Learning Research* 12 (2011), pp. 2825–2830 (cited on page 27).